Extensional forearc structures at the transition from Alaska to Aleutian Subduction Zone: slip partitioning, terranes and large earthquakes

Amin Kahrizi, Matthias Delescluse, Nicolas Chamot-Rooke, Manuel Pubellier, Anne Bécel, Donna Shillington, Mladen Nedimović, Cédric Bulois

INSTITUT DE FRANCE
Académie des sciences

Comptes Rendus

Géoscience

Sciences de la Planète

Amin Kahrizi, Matthias Delescluse, Nicolas Chamot-Rooke, Manuel Pubellier, Anne Bécel, Donna Shillington, Mladen Nedimović and Cédric Bulois

Extensional forearc structures at the transition from Alaska to Aleutian Subduction Zone: slip partitioning, terranes and large earthquakes

Published online: 25 July 2023

https://doi.org/10.5802/crgeos.225

Part of Special Issue: Geodynamics of Continents and Oceans – A tribute to Jean Aubouin

Guest editors: Olivier Fabbri (Université de Franche-Comté, UMR CNRS 6249, Besançon), Michel Faure (Université d'Orléans-BRGM, UMR CNRS 7325, Institut des Sciences de la Terre, Orléans), Laurent Jolivet (Sorbonne Université, ISTeP, UMR 7193, Paris) and Sylvie Leroy (Sorbonne Université, CNRS-INSU, ISTeP, Paris)

Les Comptes Rendus. Géoscience — Sciences de la Planète *sont membres du Centre Mersenne pour l'édition scientifique ouverte*
www.centre-mersenne.org
e-ISSN : 1778-7025

Comptes Rendus
Géoscience — Sciences de la Planète
Published online: 25 July 2023
https://doi.org/10.5802/crgeos.225

Geodynamics of Continents and Oceans – A tribute to Jean Aubouin

Extensional forearc structures at the transition from Alaska to Aleutian Subduction Zone: slip partitioning, terranes and large earthquakes

Amin Kahrizi [a], Matthias Delescluse [*, a], Nicolas Chamot-Rooke [a], Manuel Pubellier [a], Anne Bécel [b], Donna Shillington [c], Mladen Nedimović [b, d] and Cédric Bulois [a]

[a] Laboratoire de Géologie, Ecole Normale Supérieure, CNRS UMR 8538, PSL University, Paris, France

[b] Lamont-Doherty Earth Observatory of Columbia University, Palisades, NY, USA

[c] School of Earth and Sustainability, Northern Arizona University, Flagstaff, AZ, USA

[d] Dalhousie University, Halifax, NS, Canada

E-mails: kahrizi_amin@hotmail.com (A. Kahrizi), delescluse@geologie.ens.fr (M. Delescluse), rooke@geologie.ens.fr (N. Chamot-Rooke), manupub.pubellier@gmail.com (M. Pubellier), annebcl@ldeo.columbia.edu (A. Bécel), donna.shillington@nau.edu (D. Shillington), mladen@ldeo.columbia.edu (M. Nedimović), bulois@geologie.ens.fr (C. Bulois)

Abstract. The Unimak and Shumagin segments of the Alaska Aleutian Subduction Zone show extensional deformation of the forearc since the Miocene. Using legacy seismic profiles and modern multichannel seismic data, we update the structural map of the area, focusing on the intersection between trench-parallel, landward-dipping normal faults rooting in the plate interface and trench-oblique to trench-perpendicular normal faults, all showing signs of recent activity. We investigate for the first time the origin of the trench-parallel extension and explain the horsetail geometry of the Central Sanak Basin as the termination of a slip-partitioning right-lateral strike slip fault. Re-analysis of subduction zone thrust earthquakes slip vectors indicates a possible onset of slip partitioning in the vicinity of the Central Sanak Basin. In the hypothesis of a continuum of deformation, finite deformation from normal fault offsets show a slow sliver motion of less than 1 mm/yr, which is below the resolution of GNSS measurements. Both trench oblique and trench parallel faults have been cited as reactivated terrane sutures, the presence of which may act as upper-plate weaknesses needed to allow slip partitioning in a context of low convergence obliquity. Weak landward-dipping normal faults rooting in the plate interface have also been linked to the tsunamigenic rupture of the shallow plate interface. We infer that the trench parallel Unimak Ridge, associated with the 1946 Mw 8.6 tsunami earthquake, is the last expression of terrane sutures reactivation before their westward vanishing in the more recent Aleutian arc.

Keywords. Alaska Subduction Zone, Forearc, Seismic reflection, Terranes, Slip partitioning, Megathrust earthquakes, Tsunamis.

Published online: 25 July 2023

* Corresponding author.

1. Introduction

Within the upper plate of subduction zones, forearcs deform in reaction to a variety of processes occurring during the convergence between two tectonic plates. A classic example is the indentation of the margin by the subduction of seamounts from the downgoing plate [e.g. Dominguez et al., 1998]. The varying basal and internal friction at the base and within the wedge, in addition to accretion or underplating of incoming sediments, can also destabilize the slope and lead to extension or compressional deformation of the forearc [Dahlen et al., 1984, Lallemand et al., 1994, Cubas et al., 2013]. In non-accretionary margins, basal erosion [von Huene and Lallemand, 1990, von Huene and Scholl, 1991, Clift and Vannucchi, 2004] due to rough oceanic basement and hydrofracturing [e.g. Le Pichon et al., 1993] often leads to subsidence and extension of the forearc (e.g. Figures 1 and 2), although uplift and compression are also possible [e.g. Noda, 2016]. Independently of these processes, strike slip deformation can occur due to slip partitioning of oblique convergence between two plates [e.g. McCaffrey, 1992], leading to the trench-parallel motion of a so-called sliver block with respect to the arc.

All these factors relate to time scales much larger than the seismic cycle, and it is thus difficult to correlate forearc structures with downdip variations of the seismogenic behaviour of the plate interface [Hyndman et al., 1997, Oleskevich et al., 1999] or segmentation of large earthquake ruptures [e.g. Kelleher and McCann, 1976]. Nevertheless, several studies showed some worldwide spatial correlations between features in residual gravity anomalies, a proxy for tectonic structures of forearcs and downgoing plates, and large earthquake rupture zones [Song and Simons, 2003, Wells et al., 2003, Bassett and Watts, 2015]. The underlying processes at work are however still debated and another approach is to look for some short-term feedback on specific structures after the occurrence of large earthquakes. Tsuji et al. [2011, 2013] imaged an active landward-dipping normal fault bounding a half-graben just landward of the shallow rupture zone of the tsunamigenic 2011 Mw 9.0 Tohoku megathrust earthquake. McKenzie and Jackson [2012] further showed the systematic occurrence of extensional aftershocks in the forearc following megathrust earthquakes with a large shallow plate interface slip. Both groups associate landward-dipping normal faults to the "overshoot" mechanism [e.g. Ide et al., 2011] in which amplified slip on the shallow plate interface may be due to the release of gravitational potential energy [McKenzie and Jackson, 2012] along a weak landward-dipping normal fault. Consequently, detecting such landward-dipping normal faults in other subduction zones is of particular interest for the study of tsunamigenic hazard [e.g. Bécel et al., 2017].

The Unimak and Shumagin segments of the Alaska-Aleutian Subduction Zone (hereafter AASZ) (Figure 1) have long been recognized as a transitional domain between two contrasting subduction regimes, as these segments encompass the transition from an oceanic–oceanic subduction along the Aleutian arc to an oceanic–continental subduction along the Alaska Peninsula [e.g. Scholl et al., 1975, Lewis et al., 1988], accompanied by a westward increase in the slab dip angle [Hayes et al., 2018, Kuehn, 2019] and a contrasted history of terranes docking (Figure 1). This makes the Unimak and Shumagin segments particularly suited to study the possible influence of forearc structures on the short-term behaviour of the plate interface, in particular when compared to the neighboring Semidi segement: From the Shumagin to the Unimak segment of the AASZ, seismic profiles consistently show landward-dipping, trench-parallel normal faults [Figures 1 and 2; Bruns et al., 1987, von Huene et al., 2019, Bécel et al., 2017] controlling the development of half-grabens in the forearc. A deep seismic reflection profile shot over the Shumagin segment shows one major landward-dipping fault rooting at 35 km depth in the plate interface (Figure 3) possibly indicative of tsunamigenic, shallow ruptures coeval with megathrusts earthquakes [Bécel et al., 2017]. Indeed, in the Unimak segment of the AASZ [Figure 1; Miller et al., 2014], the landward-dipping normal fault in the upper plate may influence the seismicity [von Huene et al., 2012] and follows the rupture zone of the 1946 Mw 8.6 Unimak tsunami–earthquake [Johnson and Satake, 1997, López and Okal, 2006, Okal and Hébert, 2007, von Huene et al., 2012]. This tsunami earthquake features, by definition [Kanamori, 1972], a shallow rupture zone. Like the Unimak segment, the Shumagin segment (Figure 1)—also known as the Shumagin Gap [Davies et al., 1981]—is thought to be poorly locked [Figure 1B; Fournier and Frey-

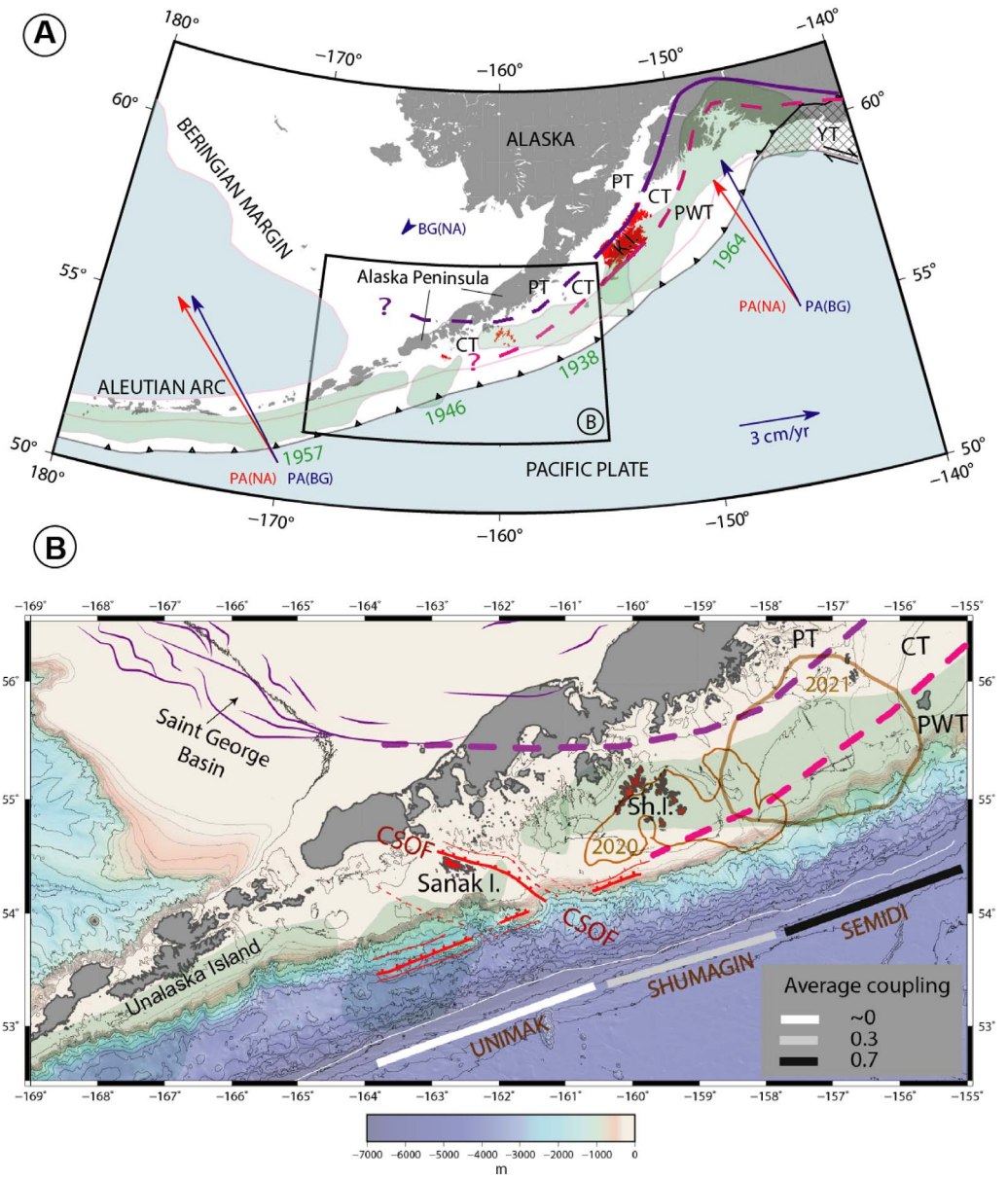

Figure 1. The Alaska-Aleutian Subduction Zone (AASZ). (A) Overview. Main terrane sutures between Prince William Terranes (PWT) and Chugach Terrane (CT, from the geology of islands in red) (dashed pink line) and between Chugach and Peninsular Terrane (PT), respectively south and north of the dashed purple line. Rupture zones of large 20th century earthquakes from aftershocks are shown in green [Tape and Lomax, 2022]. Pacific/North-America and Pacific/Bering Plate convergence vectors as well as Bering/North America motion are from GSRM v2 [Kreemer et al., 2014]. YT: Yakutat Terrane. K.I.: Kodiak Island. (B) Detailed view of the Unimak, Shumagin and Semidi segments. Addition of rupture zones (slip > 0.5 m) of the 2020 Mw 7.8 Simeonoff [thin brown contour from Liu et al., 2020] and 2021 Mw 8.2 Chignik (thick brown contour, https://earthquake.usgs.gov/earthquakes/eventpage/ak0219neiszm/finite-fault) megathrust earthquakes. Average coupling on the segments are simplified from Li and Freymueller [2018] and Briggs et al. [2023]. Simplified extensional structures from Bruns et al. [1987] are shown in red. Sanak I.: Sanak Island. Sh.I: Shumagin Islands. CSOF: Central Sanak oblique faults.

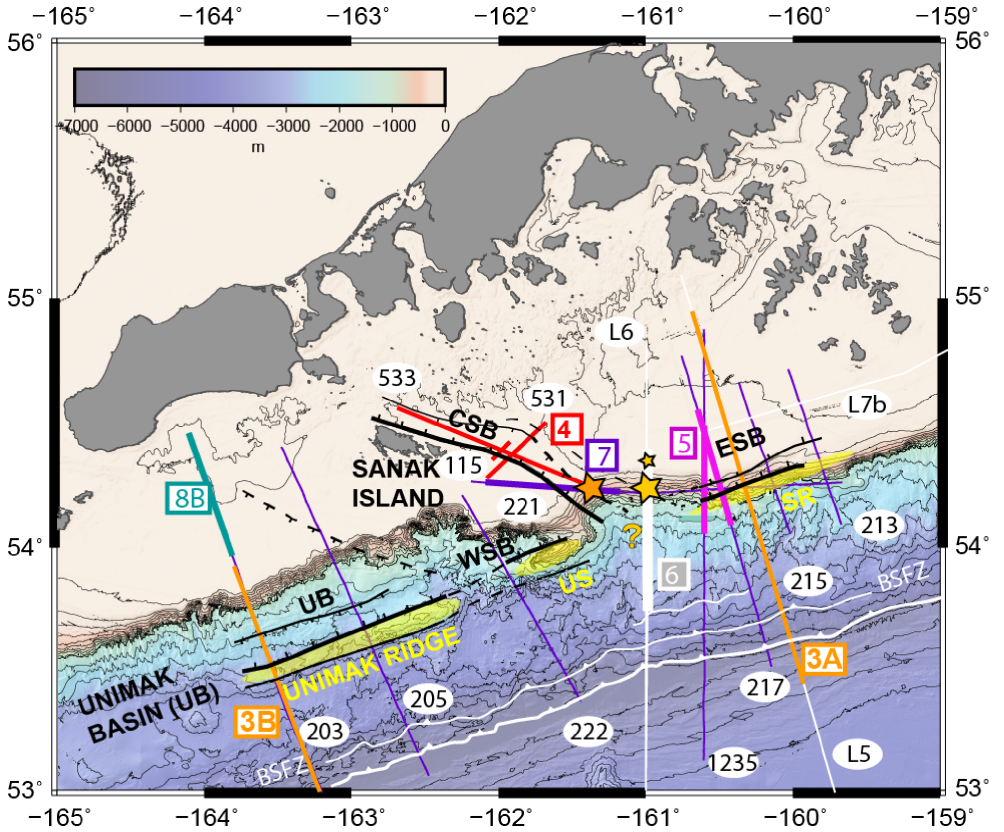

Figure 2. Main seismic lines used in this study, named in white ellipses. Black normal faults are simplified from Bruns et al. [1987]. White thrust lines represent the trench and the Backstop Splay Fault Zone (BSFZ) delimiting a narrow accretionary wedge from the margin framework (see text). The yellow question mark locates the area of shelf edge embayment which had poor seismic coverage in Bruns et al. [1987] and Horowitz et al. [1989]. Numbers in colored squares indicate Figure numbers next to profiles of the same color. Stars indicate basement highs not aligned with trench parallel ridges shaded in yellow: Unimak Ridge; Unimak "Seamount" (US); Shumagin Ridge (SR). WSB: Western Sanak Basin; CSB: Central Sanak Basin; ESB: Eastern Sanak Basin.

mueller, 2007, Li and Freymueller, 2018]. In contrast, the Semidi segment, east of the Shumagin segment, is locked [Fournier and Freymueller, 2007] and does not show any landward-dipping normal fault nor half-graben basin [von Huene et al., 2016] as along the Shumagin segment. In this Semidi segment, recent earthquakes showed deep ruptures (Figure 1) in 2020 [Mw 7.8, Liu et al., 2020, Jiang et al., 2022] and 2021 [Mw 8.2, Liu et al., 2022].

Trench-parallel faulting is not the only tectonic deformation recorded in the forearc of the Shumagin segment. The oblique Central Sanak basin is located at the western boundary of the Shumagin segment (Figure 1). It is believed to follow a reactivated Beringian margin structure [Bruns et al., 1987, Lewis et al., 1988] and may correspond to the eastern end of the 1946 Unimak tsunami earthquake rupture zone [Lewis et al., 1988]. Although there are large uncertainties in the estimation of the 1946 rupture zone by aftershock relocations, no aftershocks have been relocated east of the Central Sanak basin [López and Okal, 2006]. In the Eastern Sanak Basin, the landward-dipping normal fault may also reactivate a pre-existing suture between accretionary terranes that form the overriding plate [Shillington et al., 2022]. Although both oblique and trench-

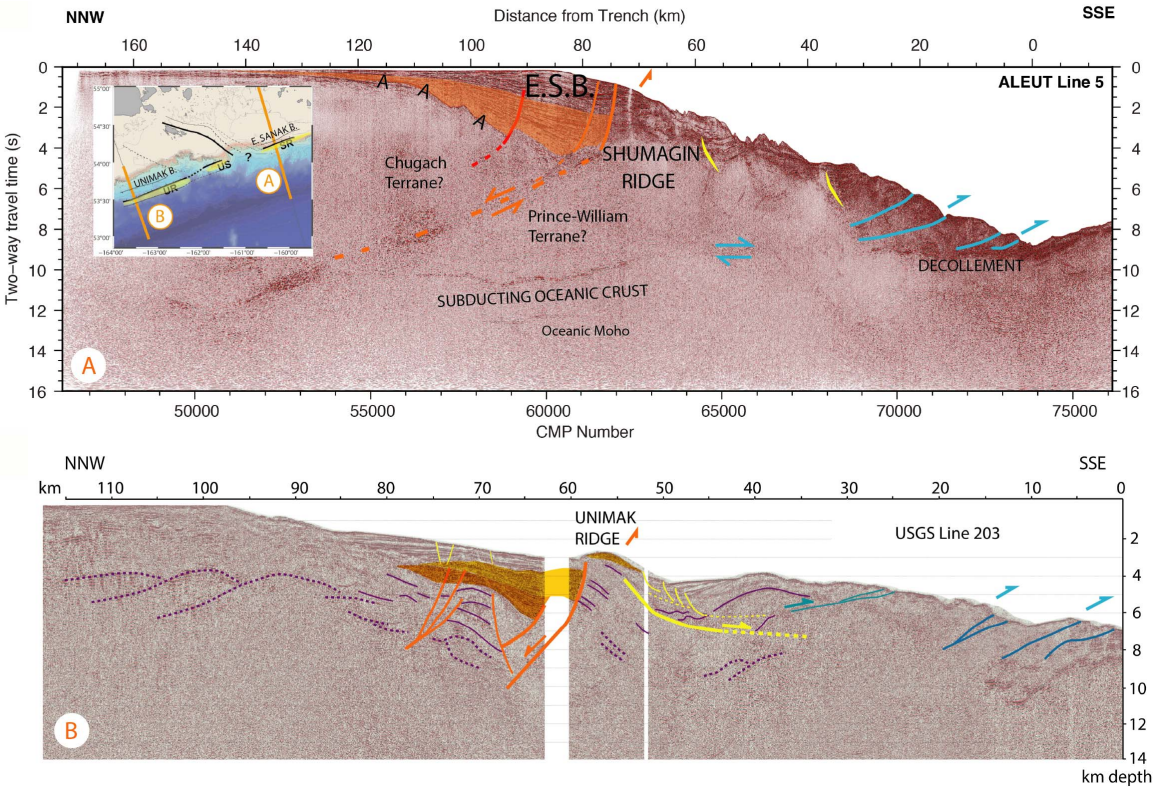

Figure 3. Major landward dipping normal faults flanking (A) Shumagin Ridge and (B) Unimak Ridge (B). Colored arrows illustrate the possible "overshoot mechanism" (see text) linking shallow subduction interface rupture and landward-dipping normal faults. (A) Time-migrated ALEUT Line 5 modified from Bécel et al. [2017]. See inset for location. Orange landward normal fault branches bounding the buried Shumagin Ridge merge in the deep landward reflector rooting in the plate interface. The transparent orange wedge in the Eastern Sanak Basin (E.S.B.) shows the Miocene syn-extension sediments. Horizon A is the tilted Eocene-eroded paleo-shelf. Yellow dashed lines indicate a few seaward normal faults, while blue faults are splay faults and thrusts in the near-trench area. Vertical exaggeration is 2 in the sediments and around 1 below basement. (B) Depth converted poststack time migration of USGS line 203 modified from Miller et al. [2014]. Purple reflectors are interpreted as pre-extension. The orange and yellow wedges are syn-extension sediments rotated by a major landward normal fault tilting the Unimak Ridge block. Yellow lines represent seaward normal faults and decollements in weak layers. Vertical exaggeration is 2.

parallel normal faults have formed basins during the Miocene and have been described as recently active [Figure 4; Bécel et al., 2017, Bruns et al., 1987], the origin of the oblique extension has never been discussed, nor has been the relationship between the two extensional systems.

Here we use available legacy and modern multichannel seismic datasets to investigate the extensional features of the forearc in the Unimak and Shumagin segments of the AASZ. Forearc extensional faults have been known for a long time to be present in the vicinity of trenches [e.g. Aubouin et al., 1984] in response to various factors including gravity combined with vertical motion, but also forearc stretching due to arc-parallel sliver motion in oblique subduction [e.g. Avé Lallemant, 1996]. Our analysis suggests such a dual origin for forearc extension. We discuss the possible onset, or starting point, of Aleutian

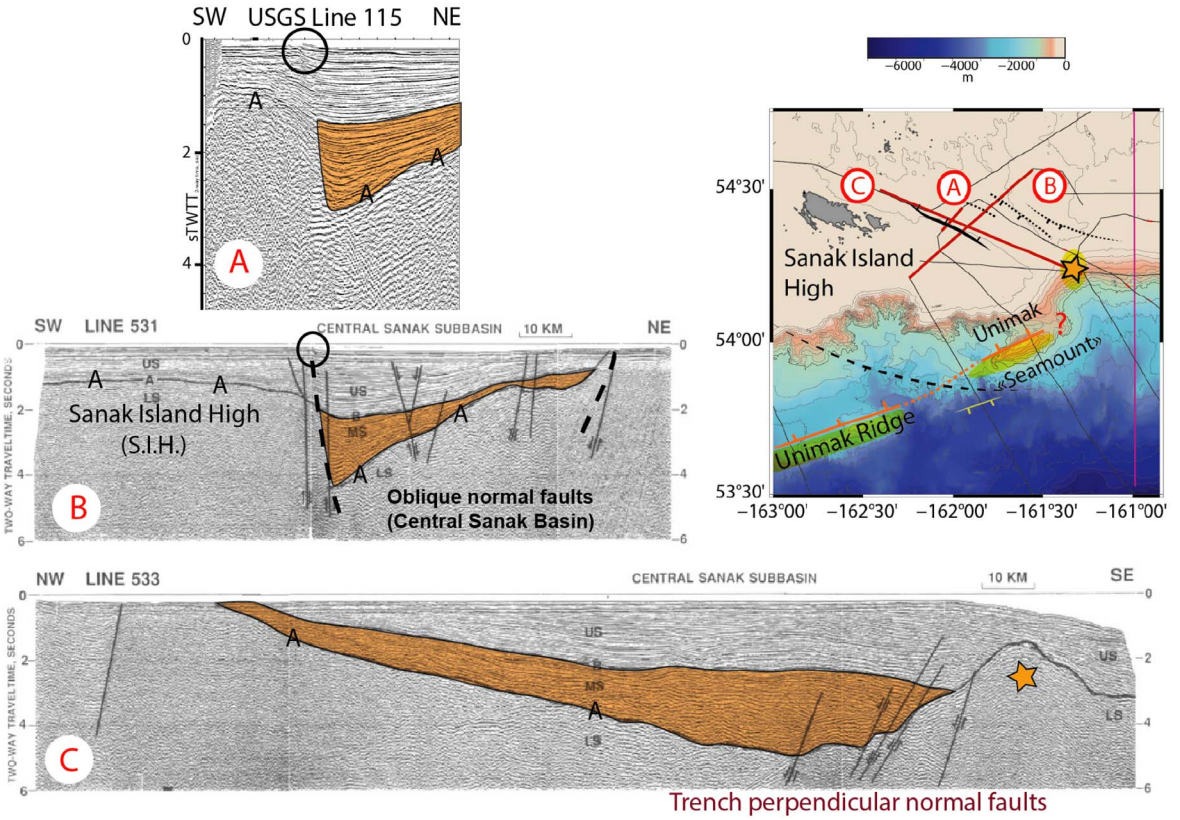

Figure 4. Structure of the Central Sanak Basin (CSB). USGS 531 and 533 modified from Bruns et al. [1987] and USGS line 115 crossing the oblique Central Sanak Basin across and along strike. See inset for location. The surface offset of the main normal fault on lines 531 and 115 is 80 m while the offset of the early Miocene horizon A is estimated around 4–5 km. Line 533 shows the basement tilt towards the SE. The basement high marked by a star is reported in the inset map and Figure 2.

partitioning around the Sanak Island and interpret the 280-km-long, landward dipping, trench-parallel normal fault system from Unimak to Shumagin segments in terms of reactivation of terrane sutures and seismogenic behaviour of the shallow plate interface.

2. Geological background

The Alaska-Aleutian Subduction Zone is an area of important seismic and volcanic activity extending from the Alaska landmass and Peninsula to the Aleutian Islands (Figure 1). It is likely that the Mesozoic and Tertiary crustal configurations still have an impact on present-day subduction zone processes. To the east, the modern subduction encompasses a segment which has a history conforming with the tectonic evolution of the cordilleras of North America dating back from the Jurassic [Dickinson, 2004], whereas to the west an island arc formed to the south of the Aleutian Basin [Scholl et al., 1987, Lewis et al., 1988, Lonsdale, 1988, Vallier et al., 1994]. The US and Canadian western margins are well known to have been constructed by the collage of a number of accreted exotic terranes originated from collision around the Paleo-Pacific and the modern Pacific basins. These terranes were in large part translated along the north American margin by long right-lateral wrench faults [Davis et al., 1978, Monger and Irving, 1980, Coney et al., 1980]. Such terrane docking processes resulted in the Cretaceous accretion of the Wrangellia–Peninsular Terrane, and more recently the Paleogene accretion of the Chugach, Prince William, and Yakutat terranes [Figure 1; Plafker and Berg, 1994, Plafker et al.,

1994, Garver and Davidson, 2017]. The docking of the Wrangellia–Peninsular terranes created an orogen that extended to the north, beyond the South Alaskan margin, along the Beringian shelf during the Late Cretaceous. The convergence and the subduction zone were abandoned during the Late Cretaceous (Maastrichtian) and sealed by Paleogene deposits [Worrall, 1991, Bruhn et al., 2004]. Relics of the orogen are present as compressive structures, interpreted from the gravity field under the shelf as well as from seismic profiles and velocity models [e.g. Horowitz et al., 1989, Shillington et al., 2022].

After the Late Eocene, subduction resumed along the present-day Aleutian Arc system, as shown by Oligocene and Early Miocene volcanics and thick sedimentary deposits in the forearc basin. The trace of the Beringian suture zone is likely to be marked by the deeply sedimented St George–North Aleutian basins (St George Basin in Figure 1B), supporting that the terranes follow the abandoned Beringian margin [Lewis et al., 1988, Lizarralde et al., 2002; Figure 1] west of the Shumagin segment. The Shumagin and Unimak areas are located at the termination of the Alaskan Peninsula where the Aleutian arc splays out of the Alaskan Shelf. This area is marked by a drastic change of the present day configuration of the subduction zone which shows a sharp change from a thick crust and a large forearc to a narrower margin (Figure 1). Transverse structures such as the Central Sanak Basin (CSB in Figures 2 and 4) mark the boundary and have an orientation which parallels the former Cretaceous margin, and therefore the intrinsic structure of the continental margin may have experienced reactivation.

Around the present-day shelf edge, trench-parallel basins extend from west to east of the oblique CSB: the Unimak, Western Sanak and Eastern Sanak basins respectively (Figure 2). All basins are filled with Miocene to Holocene sediments above a tilted paleoshelf that was eroded from Oligocene to Miocene [Bruns et al., 1987]. This tilted acoustic basement is ubiquitous in seismic profiles (horizon A, see Figures 3 and 4). The paleoshelf has a refraction velocity of 4.5 km/s and, from nearby island geology, this paleoshelf basement is inferred to include Paleogene intrusive, arc-affinity rocks [Bruns et al., 1987] extending down-slope to the backstop splay faults zone (BSFZ) which is also the accretionary wedge backstop [Figure 2; von Huene et al., 2020]. Landward-dipping normal faults bound the trench-parallel half-graben basins seaward. Their footwall marks a linear ridge, which is exposed in the Unimak basin (Unimak Ridge, Figures 2 and 3B) but remains buried by the sediments of the Eastern Sanak Basin (Shumagin Ridge, Figures 2 and 3A).

In the Eastern Sanak basin (ESB), reflections from the main landward-dipping normal fault have been imaged down to the plate interface at 35 km depth [Bécel et al., 2017; Figure 2]. In a recent deep seismic refraction study, Shillington et al. [2022] showed that the hanging-wall block has a higher P-wave velocity than that of the seaward footwall block which includes the ridge. These authors interpret the fault as a former thrust separating the Chugach Terrane from the Prince William Terrane. It likely corresponds to a suture previously mapped south of the Kodiak Island and extrapolated westward towards and beyond the Shumagin Islands [Moore et al., 1983]. It is thus tempting to consider the landward flank of the Aleutian-arc-parallel Unimak Ridge to be the continuation of the Eastern Sanak landward normal fault [von Huene et al., 2019]. However, the terranes-related structures are supposed to bend and follow the NW–SE Beringian margin geometry rather than run along the Aleutian Arc [Lewis et al., 1988; Figure 1], in apparent contradiction with the Shumagin and Unimak trench-parallel ridges being connected and having a common geological origin (Figure 4).

Indeed, it is the oblique Central Sanak basin that is interpreted as a reactivation of the Beringian margin structures [Bruns et al., 1987, Lewis et al., 1988]. Onlaps and unconformities within all sub-basins point to a Miocene onset of extension on the normal faults, whether they are trench-parallel or reported to follow the Beringian margin orientation (Figures 3 and 4). All Sanak basins show recent—although moderate—activity of both trench-parallel and oblique normal faults [Bruns et al., 1987, Bécel et al., 2017]. As a result, this raises questions about the nature of the extension activating the diversely oriented structures, how the two basin families interact at their intersection (Figure 2) and subsequently whether forearc structures can provide a window into controls on modern deformation and seismogenesis in this area of the AASZ.

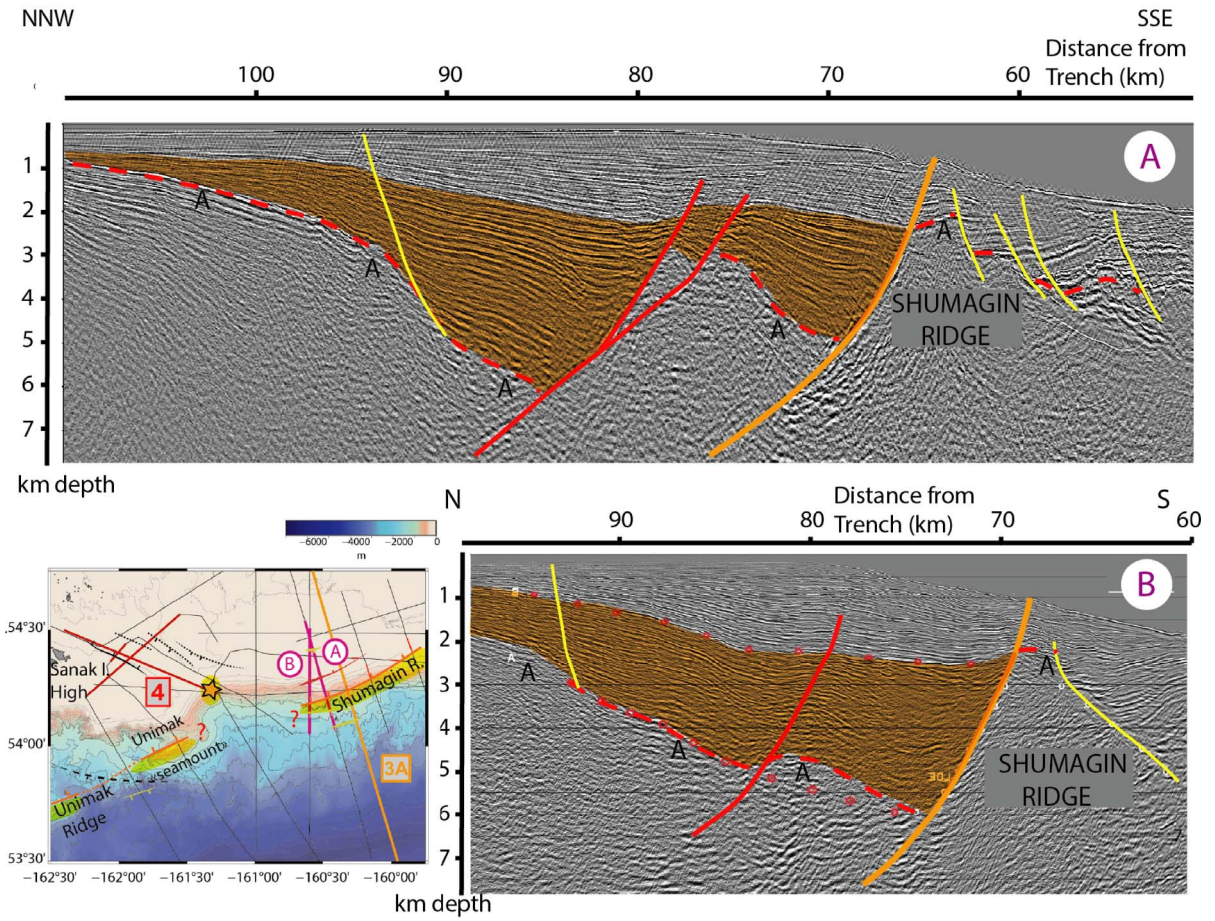

Figure 5. Structure of the Eastern Sanak Basin (A) USGS line 217 Prestack Depth Migration (PSDM), modified from von Huene et al. [2019]. (B) Reprocessed R/V Ewing line 1235, modified from von Huene et al. [2019]. Orange fault is the main Sanak landward-dipping fault, red fault the "secondary" fault and yellow faults are seaward-dipping normal faults. Colored sediments are Miocene sediments above the basement horizon A. Vertical exaggeration is 2.

3. Data and methods

Many seismic profiles used in this study were acquired in the 70's and 80's and reflection images derived from these data are published in Bruns et al. [1987] and Horowitz et al. [1989]. These authors built isopach maps of the basins fill and interpreted the locations of the main border normal faults (see a simplified version in Figures 1 and 2 and the Horowitz et al. map in Supplementary Figure S1). Although there has not been a major improvement in density of profiles since the earlier studies of Bruns et al. [1987] and Horowitz et al. [1989], some of the legacy data have been reprocessed [Miller et al., 2014, von Huene et al., 2019; Figures 3 and 5] and some new deep penetration profiles acquired with an 8-km-streamer are available from the ALEUT experiment [Shillington et al., 2011, Li et al., 2018, Bécel et al., 2017]. ALEUT Line 6 (Figure 6) is of particular interest since it is located at the junction of the Central and Eastern Sanak basins, in an area of poor coverage of the legacy data. The shelf break and slope section of Line 6 has been reprocessed using the CGG Geovation Seismic Imaging software. The processing workflow includes denoising, SRME and Radon multiple attenuation and finally Kirchhoff Prestack Time Migration [see Liang et al., 2019, for more details on the processing workflow]. USGS Line 221 was available as a non-

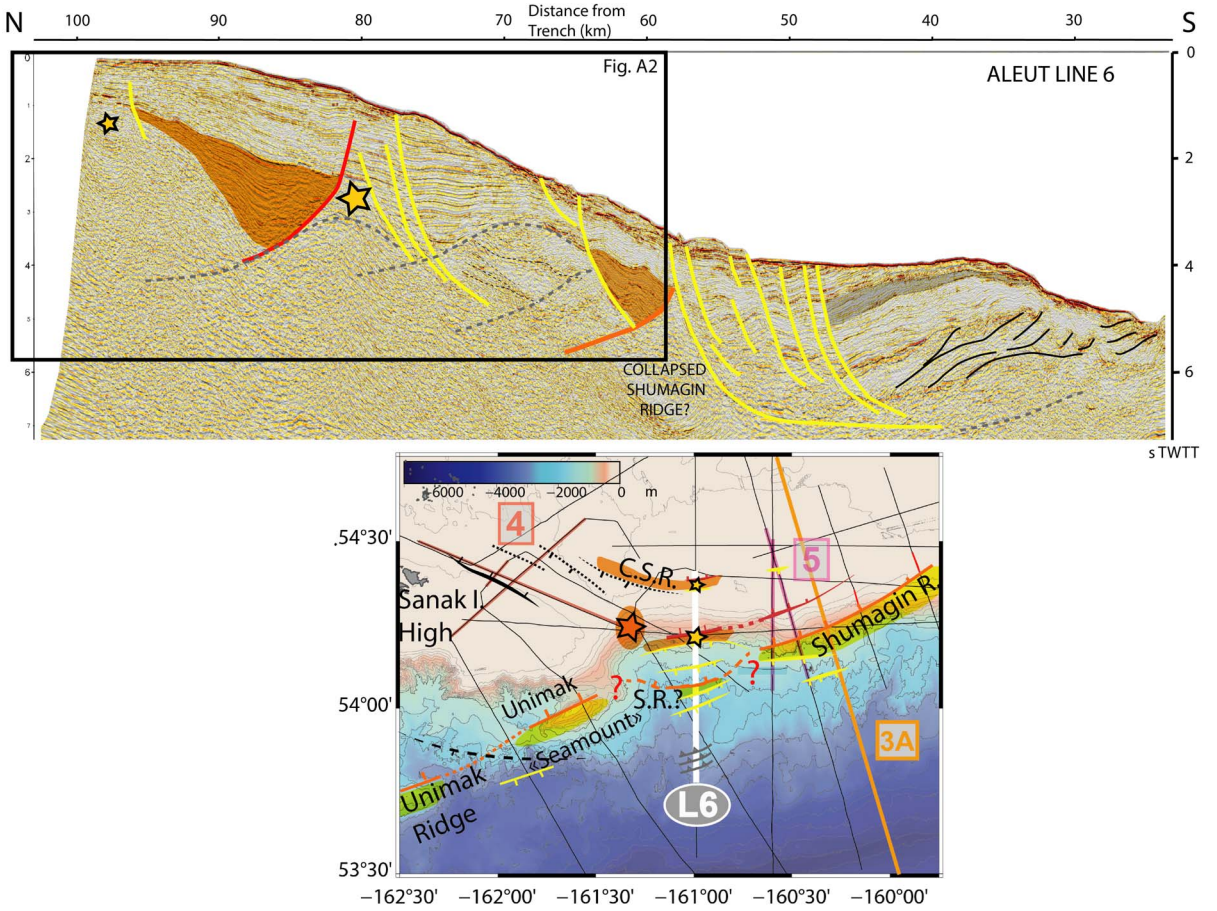

Figure 6. Upper slope and slope structure at the intersection between Central Sanak Basin and Eastern Sanak Basin: Reprocessed ALEUT Line 6 and interpretation. The black frame locates the Prestack Depth Migrated image (PSDM) and streamer tomography velocity model in Supplementary Figure S2. Orange shaded areas show Miocene sediments recording clear activity of the landward normal faults (red and orange). Yellow faults are all seaward normal faults. Black lines represent the toe-thrust fault system downslope while grey shaded areas record the tilting of the block. Dashed grey lines show weak basement reflectivity tentatively interpreted as old thrust structures from former accretionary prism or within terranes. C.S.R.: Central Sanak Ridge; S.R.: Shumagin Ridge.

migrated stack but is presented here after application of a post-stack, water velocity Kirchhoff Migration (Figure 7).

Streamer tomography (Supplementary Figure S2), as published in Bécel et al. [2017], is also used to detect a basement high beneath the shelf (small yellow star on Figure 2, 100 km from the trench in Figure 6). This high was found difficult to image by conventional processing of the reflectivity. Long-streamer refracted first arrivals confirm the 4.5 km/s *P*-wave velocity of the basement reported by Bruns et al. [1987] (horizon A interpreted as the eroded paleoshelf). This localized shallow high velocity delimitates a horst or ridge structure that was neither detected in previous studies, nor interpreted in Bécel et al. [2017].

The final structural map of the basins (Figure 8, with faults coordinates in Supplementary Material) also uses constraints from the vertical gradient of the free-air gravity anomaly from DTU13 [Andersen et al., 2015] as well as the Analytic Signal (AS) extrema [as described in Mickus and Hinojosa, 2001, Saad,

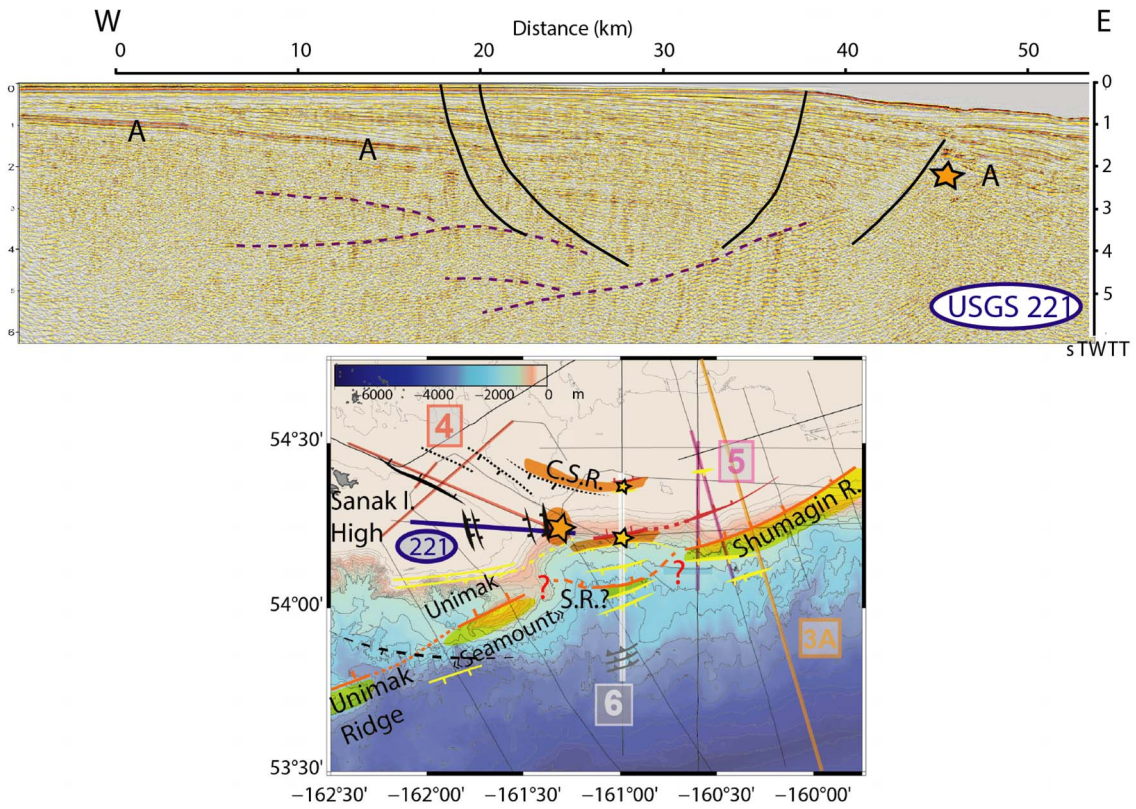

Figure 7. The Central Sanak Basin South Graben. Post-stack migrated USGS line 221. Black faults are trench-perpendicular normal faults (see map), misplaced in the simplified structural trend of Figure 2. Purple dashed lines are interpreted to be former margin low-angle thrusts. Notice the eastward tilt of the basement horizon A. Orange star shows the same basement high visible in line USGS 533 (Figure 4). C.S.R.: Central Sanak Ridge; S.R.: Shumagin Ridge.

2006, Dung and Thanh, 2016] in order to discuss the lateral continuity of the basement structures seen in 2D seismic profiles (Supplementary Figures S3 and S4). In this study, we map faults that have clearly been active since the Miocene with attested [Bruns et al., 1987, Bécel et al., 2017] or suspected continued activity up to the present. However, we are not able to quantify the variation of the faults activity through time due to the lack of wells and complex sedimentary processes around forearc faults [e.g. Calvès et al., 2017, Ratzov et al., 2010]. In Figures 3 to 7, faults are sometimes not drawn in recent sediments as their activity is not clearly recorded there, which can be the result of a regional 4-fold increase in sedimentation rates from Pliocene to present [von Huene and La Verne, 1973, ODP]. It is thus important to notice that the apparent decrease in the sedimentary record of faults activity after the Miocene (e.g. Figure 5) may be an artifact of the competition between sedimentation and tectonics, as some clear fault scarps are attested by multibeam bathymetry [Bécel et al., 2017].

4. Interpretation results

4.1. *Landward-dipping normal faults*

Figure 3 shows two profiles (USGS 203 and ALEUT 5) representative of the forearc basin structures of the Unimak and Eastern Sanak basins, respectively. The sub-basement imaging of ALEUT line 5 indicates

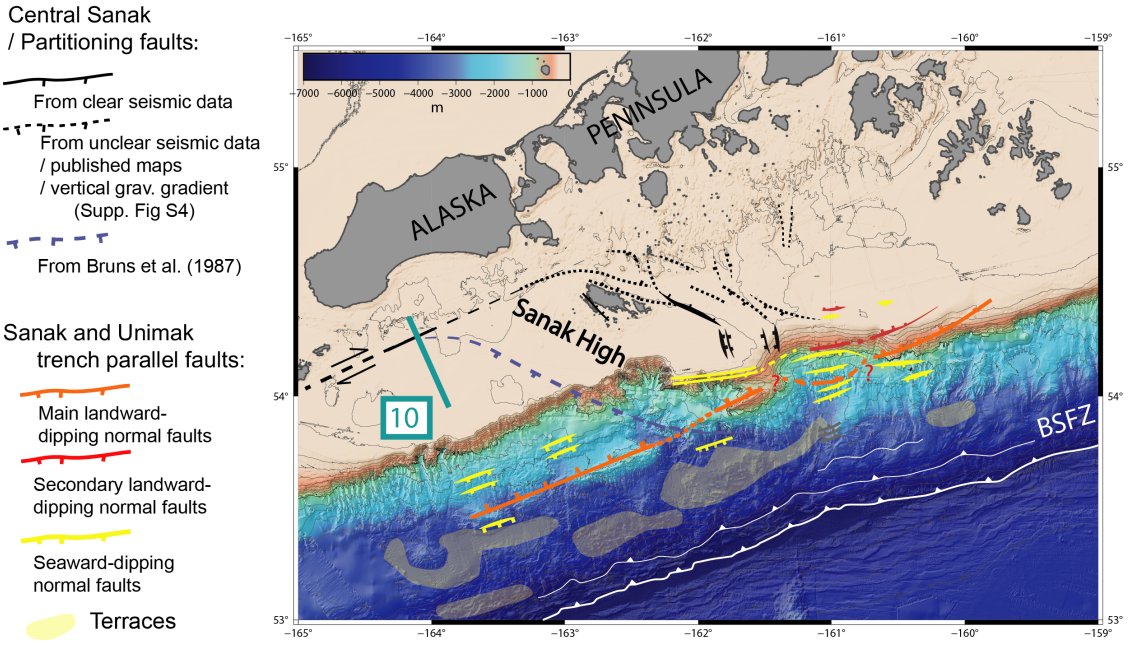

Figure 8. Final structural map of the Unimak and Shumagin segments of the AASZ. Black faults represent partitioning-related oblique and trench perpendicular faults revealing a horsetail structure at the onset of slip partitioning. White thrusts show the trench and the BSFZ (Backstop Splay Fault Zone). Digitized faults are available in Supplementary Material.

that only one of the shallow landward-dipping normal fault branches connects to the deep landward-dipping reflector (~75 km from the trench) [Bécel et al., 2017, Shillington et al., 2022], while another landward-dipping normal fault ~20 km NNW (and ~95 km from the trench) appears to root at shallower depth. This 20-km-wide block between the two landward normal faults is not easy to detect in the legacy data, except in the reprocessing by Miller et al. [2014] and von Huene et al. [2019], where the "secondary" trench-parallel landward-dipping fault is clearly confirmed all along the Eastern Sanak basin, and particularly in profile 217 (Red fault in Figure 5).

ALEUT line 6 (Figure 6) runs at the junction between the trench-parallel Eastern Sanak Basin and the oblique Central Sanak Basin, in an area of local shelf break embayment (Figure 2). In comparison with the eastern trench perpendicular lines (e.g. ALEUT 5, USGS 217, see Figure 3 and 5), we observe a more complex basement morphology (Figure 6). von Huene et al. [2019] interpret the horst immediately seaward of the shelf break (yellow star 80 km from the trench in Figure 6) as the Shumagin Ridge, but none of the basement horsts recognized in ALEUT line 6 are actually aligned with the Unimak and Shumagin ridges (Figure 2). Therefore, this observation challenges the continuity of both ridges inferred in previously published interpretations. On the other hand, the main upper slope landward-dipping fault in line 6 (red in Figure 6) may be the continuation of the aforementioned "secondary" landward-dipping fault in ALEUT line 5, USGS 217 and LDEO 1235 (red fault in Figures 3 and 5). There is however no clear evidence for a continued "main" landward-dipping normal fault (orange fault in Figure 5), and many line 6 faults, such as the numerous seaward-dipping normal faults, are difficult to identify in the eastern lines.

4.2. *Seaward-dipping normal faults*

The basement deformation is much more distributed along the ALEUT line 6 compared to the other lines. The presence of several basement horsts, including one detected by traveltime tomography (Supplementary Figure S2), implies significant activity of normal faults seaward of the Sanak basin(s) that

are not so developed in profiles to the east of ALEUT line 6 (Figures 3A and 5). Most eastern profiles indeed show half-grabens bounded by major landward-dipping faults and only a few minor normal faults farther seaward (e. g. ALEUT Line 5, Figure 3A).

Another difference is the relatively thick sedimentary pile observed from the shelf to the lower slope (Figure 5), with the seaward-dipping faults offsetting the entire sedimentary column, from seafloor to basement, without clear syn-extension wedges. In contrast, two landward-dipping normal faults are associated with the Miocene sediment wedges (just above basement in both cases). As a result, we favour a more recent activity of the seaward-dipping faults when compared to the landward-dipping faults.

Down the slope, ALEUT line 6 features a large tilted block bounded by seaward-dipping growth normal faults and landward-dipping toe-thrust faults (Figure 6). These observations all point to a slope collapse posterior to the formation of the Sanak Basin. In the entire legacy and modern dataset, such a slope-collapse is observed in a limited area in the vicinity of the shelf break embayment (Figure 6), corresponding to the junction between the oblique Central Sanak Basin and the Eastern Sanak Basin.

4.3. *Trench-oblique and trench-perpendicular structures in the Central Sanak and Unimak basins*

The main NW–SE oriented fault forming the oblique half graben (Lines 531 and 115, Figure 4, simplified in map Figures 1 and 2) is clearly expressed at the center of the oblique Central Sanak Basin, halfway between the Sanak Island and the shelf break. The fault surface throw indicates clear recent activity (Figure 4). Closer to the shelf edge and slope, USGS Line 221 shows that the similarly verging normal faults (Figure 7, 18–20 km), SW-bounding the Central Sanak Basin, are not in continuity of the main NW–SE oriented fault in lines 531 and 115 (Figure 4). These faults are also not responsible for the tilt of the basement, as Horizon A is observed dipping ENE in Line 221 (Figure 7) instead of WSW in lines 531 (Figure 4). Instead, the faults bounding the basement high in lines 533 and 221 (orange star in Figures 4 and Figure 7, respectively), are likely responsible for tilting horizon A. Therefore, these faults are interpreted to be trench-perpendicular and not trench-parallel, in agreement with a steeper basement flank in line 221 (shot perpendicularly to the fault, Figure 7) when compared to the same basement high flank in line 533 (shot obliquely to the fault, Figure 4). This orientation of the near shelf edge full graben (Figure 7) matches the vertical gradient of the Satellite Free Air gravity Anomalies (Supplementary Figures S3 and S4). These trench-perpendicular structures are also reported away from the main basins using seismic profiles and gravity data (Figure 8). An intermediate NW–SE orientation of normal fault is also mapped south of the main Sanak island [Moore, 1974]. These observations highlight that the so-called "oblique" Central Sanak basin does not only feature trench-oblique structures but also diffuse trench perpendicular structures.

Another oblique structure, parallel to the ones in the Central Sanak basin, is inferred separating the Unimak basin from the Western Sanak basin in Bruns et al. [1987] (Figure 4). Multibeam bathymetry data that were not available in the 80's and now included in the GMRT v4.0 dataset [Ryan et al., 2009], show a clear offset of the Unimak ridge (Figure 4) separating it from the "Unimak Seamount", in the continuation of the fault inferred by Bruns et al. [1987]. This offset could indicate transtensional faulting at the southwestern boundary of the "Sanak Island High" (Figure 8).

4.4. *A revised structural map of the Unimak and Shumagin segments*

Figure 8 summarizes all the observations. Compared to previous maps (e.g. Supplementary Figure S1), the reprocessed profiles and the modern ALEUT data constrain a continuous system of two landward-dipping, trench-parallel normal faults in the entire Eastern Sanak Basin (main orange and secondary red faults in Figure 8), with a more seaward location of the main (orange) landward-dipping normal fault in the "slope collapse" area of ALEUT line 6, where seaward-dipping normal faults (yellow) are numerous. The main landward-dipping fault is also offset with respect to the Unimak Seamount/Ridge, limiting the slope collapse to the intersection of the Eastern and Central Sanak basins. Many dashed lines indicate inferred faults either from other maps or

interpreted from gravity (Supplementary Figure S4) and/or unclear seismic data. The fault pattern specifically related to the Central Sanak Basin (black) is discussed in the next sections.

5. Discussion

5.1. *Nature of the trench-parallel extension in the oblique Central Sanak Basin: onset of the Aleutian strain partitioning?*

Lewis et al. [1988] and Horowitz et al. [1989] suggested that the Central Sanak Basin is part of a larger NW–SE wrench corridor re-activating the Cretaceous Beringian margin. This would require differential motion between the Alaskan Peninsula and the Aleutian arc and transtension along the paleosuture. No such motion was detected in GNSS studies of the AASZ [e.g. Li and Freymueller, 2018] and, although past re-activation cannot be ruled out, it cannot explain the present-day activity of the Central Sanak Basin. Alternatively, Bruns et al. [1987] argued that the Central Sanak Basin, and possibly the Unimak Basin, may have evolved as pull-apart basins in a trench-parallel, right-lateral strike-slip system. The northward bending of the Shumagin Formation at Sanak Island would follow a relay zone offsetting two strike-slip fault branches, the main eastern branch being either the Border Ranges Fault [Fisher, 1981] or any other terrane boundary.

A commonly invoked mechanism to explain arc-parallel extension of forearc terranes is the variation of obliquity of the subduction inherent to the non-linear shape of the arc. Increasing obliquity along arcuate forearcs contributes not only to large-scale displacement of slivers [e.g. Jarrard, 1986], but also to arc-parallel stretching and the formation of oblique basins [Ekström and Engdahl, 1989, Avé Lallemant and Guth, 1990, McCaffrey, 1992, Avé Lallemant, 1996, McCaffrey, 1996]. The onset of strain partitioning is commonly marked in the upper plate by one single deep graben more or less perpendicular to the arc, forming a wide intra-arc strait at the trailing end of the sliver. Typical well-documented examples gathered in Avé Lallemant and Guth [1990] are the Bussol Strait in the Kuril arc [Kimura, 1986, DeMets, 1992], the Semangko Graben (Sunda Strait) in the Sunda arc [Huchon and Le Pichon, 1984, Schlüter et al., 2002], and possibly the Miyako Depression in the southern Ryukyu arc [Kuramoto and Konishi, 1989]. We argue here that the Central Sanak Basin may belong to the same type of basins that find their origin in the accommodation of subduction obliquity in the upper plate at the very starting point of partitioning.

In the Aleutian arc, several canyons or passes have been identified as potential areas of localized transtension between rotating blocks translated with the sliver [Geist et al., 1988, Ryan and Scholl, 1989]. These transtensional areas mainly locate in the Central Aleutian arc and it is generally accepted that no such partitioning is active in the eastern Aleutians, the obliquity remaining below the threshold necessary to trigger sliver motion based on a balance of forces acting on the subduction thrust and the vertical shear plane [McCaffrey, 1992]. However, the analysis of the Aleutian slip vectors used to estimate the amount of obliquity led to somewhat conflicting results for the location of onset of partitioning. Ekström and Engdahl [1989] showed that slip vectors were oriented more normal to the arc everywhere west of 165° W (more or less the longitude of Unalaska Island, see Figure 1B). These authors made the striking observation that "slip partitioning appears to occur even where plate motion is nearly normal to the arc", and concluded that the strike-slip zone had to be particularly weak in the Aleutians. Using an updated centroid-moment tensor (CMT) catalog, McCaffrey [1992] proposed that similarly to the Sunda arc, a threshold value of obliquity had to be reached for partitioning to be effective, and he further estimated that this value was in the range 25–40° for the Aleutians, above the 25° value found for Sunda. At odds with Ekström and Engdahl interpretation, McCaffrey concluded to a strong upper plate.

In the last decades, GPS measurements made available for some of the islands of the Aleutian arc motivated re-examinations of the slip vector analysis [Avé Lallemant and Oldow, 2000, Cross and Freymueller, 2008]. We next discuss the implications of these and our own update of slip vectors for the arc-parallel extension around Sanak Island.

5.2. *Onset of partitioning: GPS kinematic constraints and finite deformation*

Solving simultaneously for the elastic coupling on the plate interface and the arc-velocity, Cross and

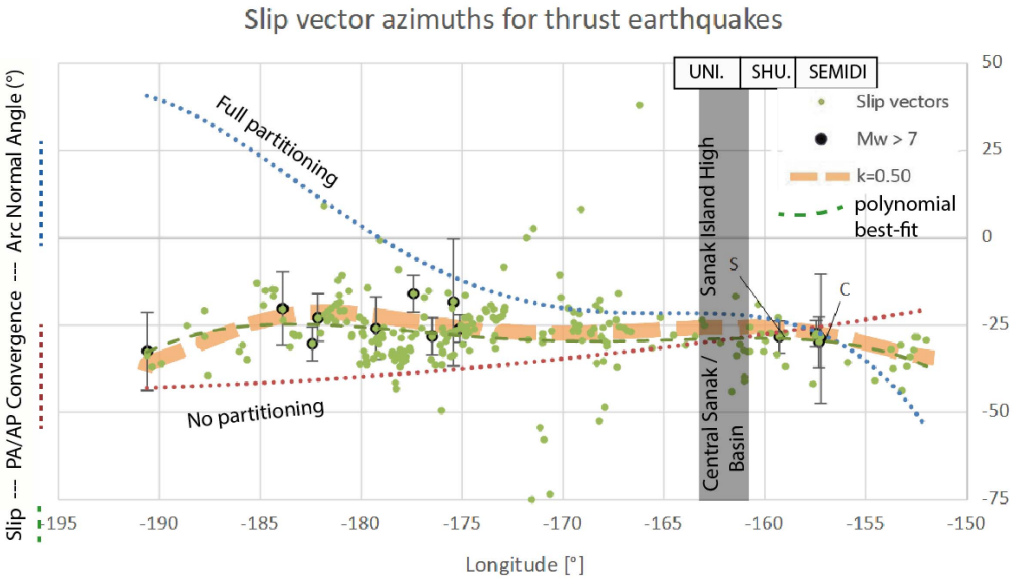

Figure 9. Azimuth plot of Mw > 5.8 thrust earthquake slip vectors extracted from the GCMT catalog [Dziewonski et al., 1981, Ekström et al., 2012] for the 1976–2022 period (hypocenter depth < 50 km and plunge tension axis >45°). Black points are Mw > 7 with uncertainties from moment tensor errors. The 2021 Mw8.2 Chignik and the 2020 Mw7.8 Simeonof megathrusts are quoted C and S respectively. Blue line is the arc-normal azimuth while the red line is the Pacific (PA)/Alaska Peninsula block (AP) convergence direction from Elliott and Freymueller [2020], corresponding to full partitioning and zero partitioning, respectively. The thick orange dashed line is the predicted slip vector azimuth in the half-partitioned case [transcurrent rate equal to half the full-partitioning rate, or $k = 0.50$; see text and Cross and Freymueller, 2008]. The grey shaded area indicates the longitude of the Central Sanak horsetail structure and the Sanak Island High (see Figure 8). See Supplementary Figure S5 for a similar figure with the Pacific/Bering convergence direction from GSRMv2 [Kreemer et al., 2014].

Freymueller [2008] include a Bering Sea plate motion in their analysis [see Li et al., 2016 for an update of the Bering block motion as well as Finzel et al., 2011, 2015]. Their model predicts active dextral strike-slip in the back-arc for the central and western Aleutians, based on significant motion of the arc with respect to the Bering Sea plate detected by GPS. East of 175° W, Cross and Freymueller [2008] show, from GPS velocities, that the arc islands virtually belong to the Bering plate and behave as a rigid block, a result confirmed by more recent studies [Li et al., 2016, Elliott and Freymueller, 2020, Xue and Freymueller, 2020]. At these longitudes, slip vectors from thrust earthquakes in the forearc are however systematically oriented between the Pacific–Bering convergence vector and the arc-normal, as in the early study of Ekström and Engdahl [1989]. The slip vectors also predict sinistral strike-slip in the forearc of Kodiak Island, in agreement with GPS and faults mapped offshore [Carver et al., 2008]. The neutral point where partitioning switches from right-lateral to left-lateral lies 158° W—east of the Shumagin Islands—suggesting that the Sanak Island may well be in the area of onset of dextral shear partitioning.

To illustrate these observations, Figure 9 is a reappraisal of the slip vector analysis using an updated catalog for the CMTs [Ekström et al., 2012] and the Pacific-Alaska Peninsula block convergence from Elliott and Freymueller [2020]. An alternative using the GSRM-v2 solution for the Pacific–Bering convergence [Kreemer et al., 2014] is presented in Supplementary Figure S5. The main difference with previous analysis is that the convergence azimuth gets closer to the arc-normal, thus predicting smaller arc-parallel motion. The pivot point remains located in the Shumagin

area, close to the 2020 Simeonof and 2021 Chignik megathrusts, so that the slip partitioning hypothesis still holds for the Central Sanak Basin. However, around the neutral point, errors in the azimuth of the slip vectors become as large as the predicted differential angle between convergence and arc-normal azimuths, so that partitioning cannot be firmly established in the Unimak segment.

The maximum rate of extension across the Central Sanak Basin can be estimated from the GPS. GPS stations on Sanak Island and those located north of the faults mapped in Figure 8 seem to belong to the same Peninsula block [Li et al., 2016, Elliott and Freymueller, 2020]. Given the quite large error ellipses, a 1 mm/yr motion cannot be excluded between Sanak Island and the Alaska Peninsula, but this is far less than the model predictions. Previous studies find a close-to-half partitioning ratio, whether a Pacific/North America convergence [0.6 in Ekström and Engdahl, 1989; 0.35 to 0.6 in Avé Lallemant and Oldow, 2000] or a Pacific/Bering convergence is considered [0.55 in Cross and Freymueller, 2008; 0.5 in Figure 9 of this study]. In this latter case, arc-parallel velocity at Sanak would be about 4 mm/yr. However, the shear rate is directly proportional to the partitioning ratio which cannot be estimated around the neutral point. Avé Lallemant and Oldow [2000] showed that this ratio is highly variable along the Aleutians, some areas being even totally non-partitioned despite highly oblique convergence. Beyond the simple analytical solutions for the critical obliquity that would trigger partitioning [Fitch, 1972, Beck, 1983, McCaffrey, 1992], numerical models show that weak zones in the upper plate control the amount of arc-parallel motion almost as much as the obliquity itself. In their Andes model, Schütt and Whipp [2020] showed that for an obliquity of 10° and a convergence of 70 mm/yr, the fore-arc moves coherently at a velocity of 1 to 2 mm/yr in the case of low strength on the shear plane accommodating the arc-parallel motion. Figure 9 suggests an obliquity of 5°–7° at Sanak Island for a 68 mm/yr convergence, in the right range for millimetric motion.

Finite deformation can be crudely estimated from the amount of slip on the normal faults bounding the Central Sanak Basin. The largest fault in seismic line 531 features a ∼5 km offset over ∼23 Myrs (the early Miocene age of horizon A, Figure 4), which leads to a minimum averaged extension rate of 0.2 mm/yr assuming a 45° dipping normal fault and a continuum of deformation until today. Considering that other faults around may contribute to extension in a more diffuse way, and a younger mid-Miocene onset of extension (15 Ma), we estimate that the maximum extension rate would hardly exceed 1 mm/yr. These motions are likely too small to be detected by GPS or quantified from slip vectors, but in the range of the numerical model predictions.

5.3. *Other structural evidences for an onset of partitioning*

The amount of arc-parallel extension around Sanak Island is hard to quantify, but putting together all the various constraints, we infer that a plausible mechanism for the formation of the Central Sanak Basin is the onset of dextral shear partitioning in a context of slowly increasing obliquity. This hypothesis requires the presence of a right-lateral strike slip fault west of Sanak Island, parallel to the islands of the arc. Some evidence for such a fault is actually found in the northernmost termination of USGS seismic line 203 (Figure 10), a seismic line crossing this potential partitioning strike slip fault area. The line shows a faulted area (from km-5 to km-25 on the profile) that may be interpreted as a flower structure, as typically found along large-scale strike-slip faults. As hypothesized by Cross and Freymueller [2008], the partitioning structures unveiled in Figure 8 are all within the forearc. This location explains the discrepancy between the GPS measurements in the Peninsula, that do not show any partitioning, and the forearc earthquakes slip vectors that do.

Active trench-perpendicular normal faults in the Central Sanak Basin (Figures 7 and 8) also call for trench parallel extension rather than the wrench reactivation of oblique Beringian structures. The finite amount of extensional deformation is kilometric up to ten kilometers at most, so that the faults remain essentially an immature horsetail-like structure at the trailing end of a nascent sliver (Figures 8 and 11). The Central Sanak Basin vanishes towards the trench slope where it interferes with extensional structures of the active margin itself, the trench acting as a free-slip boundary. The fault pattern is well reproduced in analog models of pull-apart basins [McClay and Dooley, 1995] or nascent horsetail [Basile and Brun, 1999], including the trench-perpendicular

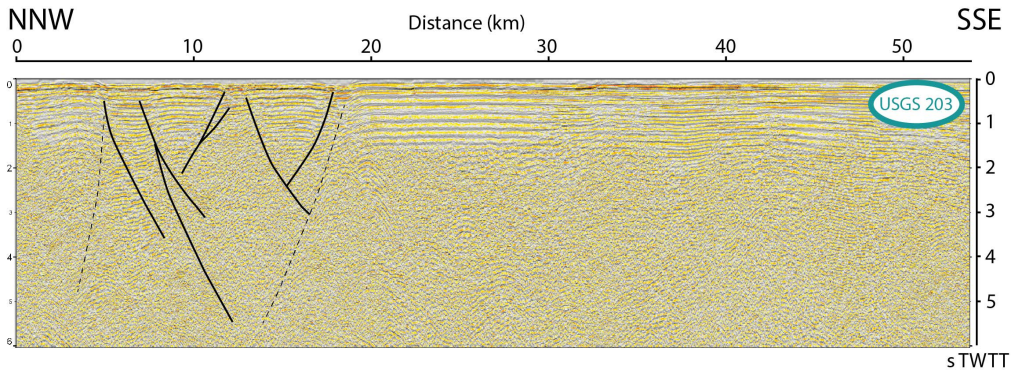

Figure 10. Non-migrated stack of the northern section of USGS profile 203 (see Figure 8 for location) with our interpretation of a flower structure where partitioning strike-slip motion is expected to localize.

faults. Multi-directional extensional faults are also documented around the Sunda Strait at the trailing edge of the Sumatra sliver, the main oblique Semangko graben interfering with slope parallel faults [Schlüter et al., 2002], or at the Hikurangi subduction zone in New Zealand [Chanier et al., 1999].

In the shelf edge area of the Central Sanak Basin, trench perpendicular normal faults are not far from landward and seaward-dipping trench parallel normal faults (Figures 7 and 8), which indicates almost equal horizontal principal stresses, leading to the predominance of the vertical principal stress, favoring gravity collapse. In this context, the discontinuities between the trench-parallel Shumagin Ridge, collapsed Shumagin Ridge, Unimak Seamount and Unimak Ridge (Figure 11) can all be interpreted as the intersection between the partitioning horsetail transtensional faults and the landward dipping normal fault system extending from the Unimak to Shumagin segments.

As discussed in the previous section, partitioning at a low angle of obliquity requires weak contacts in the forearc, which are likely present within the Chugach terranes. Transpressional terrane docking [Pubellier and Cobbold, 1996, Pubellier et al., 1996] occurred at the pivot point between a more or less convergence-normal oriented trench and a very oblique Beringian margin [Marlow and Cooper, 1980] so that around Sanak, both the Beringian sub-parallel shear-related sutures (Central Sanak horsetail, formerly Sanak "wrench zone") and frontal thrust related sutures [Shillington et al., 2022] can be reactivated nowadays (Figure 11).

5.4. *The landward-dipping normal fault system and the reactivation of terrane sutures*

Extensional deformation related to unstable slopes or general subsidence is commonly found in forearcs. Basal tectonic erosion [e.g. von Huene and Scholl, 1991] and/or underplating of sediments [e.g. Chanier et al., 1999] likely drive the long term extension in the studied area [Bruns et al., 1987] and may also explain the paired residual gravity anomaly in the Unimak segment [Figure 11, Bassett and Watts, 2015]. However, such extensional deformation rarely localises on a single structure. Although slightly offset, ridges associated with landward dipping-normal faults form a more or less 280-km-long structure running from the Unimak segment to the Shumagin segment some 60 to 80 km away from the trench (red faults in Figure 11), featuring several kilometres of vertical throw, which is quite unprecedented among the worldwide extensional forearcs. If, as discussed in the previous section, reactivation of trench-parallel thrust sutures can explain this peculiar observation, it is interesting to understand why there is no reactivation west of the Unimak segment and East of the Shumagin segment.

The western end of the Unimak Ridge, a tilted sedimentary block [Miller et al., 2014, see also Figure 3B], vanishes south-westward within the Unimak basin, in what is usually already considered to be the Aleutian-arc domain. This is also the western boundary of the Unimak tsunami–earthquake rupture zone [e.g. López and Okal, 2006; Figure 11]. Further west lies the Unalaska gap and the 1957 megathrust

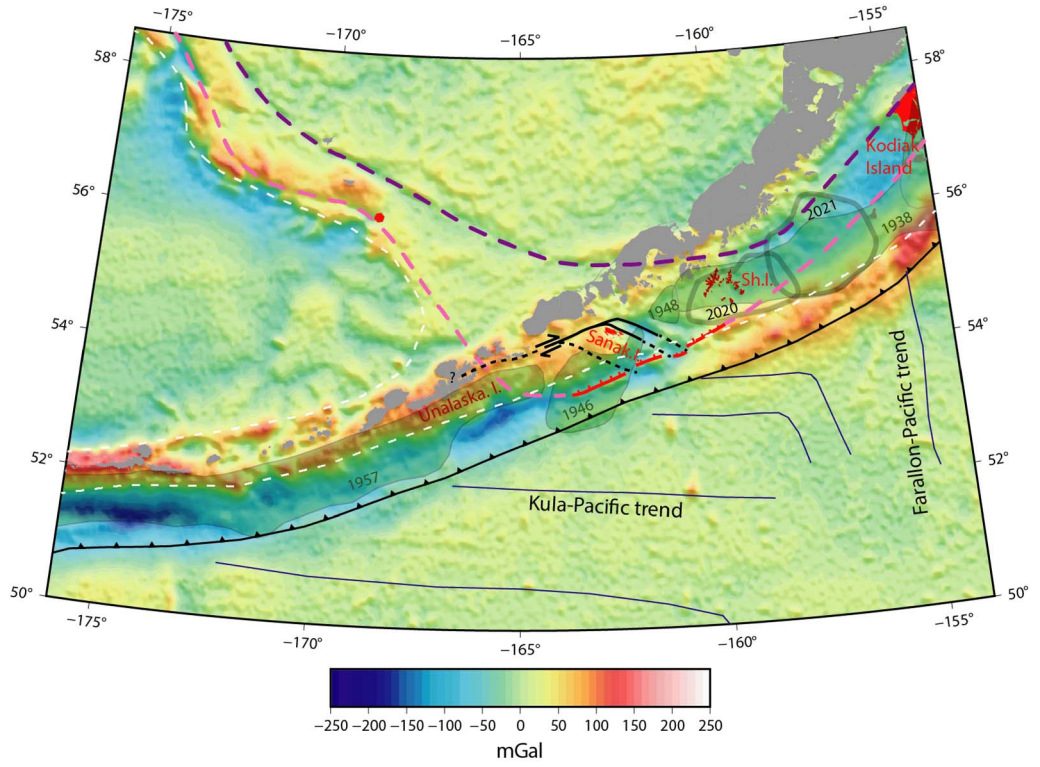

Figure 11. Synthesis map using the residual gravity anomalies of the AASZ from Bassett and Watts [2015] showing near trench and near arc polarity reversal through the Central Sanak Basin because of the slab dip angle increase towards the South-West. Large earthquake aftershocks zones in green are those from Figures 1A and B. Terrane boundaries (Chugach/PWT: pink; Chugach/Peninsular: purple) can sometimes be followed in the gravity anomalies. We propose a westward extension of the terrane boundary along the trench-parallel ridge system (in red) and a junction with the outer Beringian margin similar to Bassett and Watts [2015]. Simplified partitioning strike-slip fault and horsetail are shown, intersecting the trench-parallel ridges. The dashed continuation of the strike slip-fault toward Unalaska Island is only a guess. Red islands are reported to be part of the Chugach Terrane [Moore et al., 1983], while the red hexagon is a Beringian margin canyon where turbidites originating from rocks similar to the Shumagin Formation were dredged [Moore, 1973]. White dashed lines represent the shelf edge. Blue lines represent the orientation of magnetic anomalies (EMAG) and show the clear variation of the orientation of the subducting oceanic fabric (see text). Sh. I.: Shumagin Islands.

earthquake rupture zone (Figure 11). The southwest of the Unimak basin shows no obvious change in trench sedimentation, elastic coupling [e.g. Cross and Freymueller, 2008] or downgoing plate structure (Figure 11). As a result, it is tempting to explain the western vanishing of the Unimak ridge by the absence of pre-existing suture west of the 1946 Unimak tsunami earthquake rupture area. Figure 11 shows that it is still possible to link the western edge of the Unimak ridge with the Beringian margin as suggested in Bassett and Watts [2015]. Other previous studies do not show such a "widening" of the terrane docking area and consider a bend of the terranes around Sanak Island. However, considering the Sanak Island High (Figure 8) as the western limit of the terranes does not explain the presence of the Unimak Ridge and its virtual alignment with Unimak Seamount and Shumagin Ridge (Figure 11). Besides, Horowitz et al. [1989] report thrust structures similar to those seen beneath the Central Sanak Basin (Figure 7), but in the

Unimak segment (Supplementary Figure S1), which would indicate that the Unimak basin and ridge were once part of the former margin too.

At the eastern end of the landward-dipping normal fault system, Shillington et al. [2022] show the reactivation of a major thrust suture zone within the terranes. This suture zone is expected to extend off Kodiak Island (Figure 11) but normal faulting reactivation actually vanishes just west of the Shumagin Islands (Figure 11). A possible explanation is that the distance between the major terrane suture and the trench becomes too large (Figure 11) to allow the "overshoot mechanism" [Ide et al., 2011, Tsuji et al., 2011, McKenzie and Jackson, 2012] activating the landward-dipping fault-planes and allowing rupture of the shallow interface as during the archetypal 1946 Unimak tsunami earthquake or the 2011 Tohoku megathrust earthquake.

To further illustrate the possible link between the shallow interface behaviour and the normal reactivation of the terrane thrust sutures, mid-slope terraces are also observed trenchward of the Unimak and Sanak Basins, along the 280-km-long section of trench-parallel ridges (Figure 8). These terraces are located up-slope of near-trench reverse splay faults [BSFZ in von Huene et al., 2020, see also Figure 8] separating the margin framework from small frontal wedges. The epicenter of the 1946 Unimak tsunami earthquake is believed to be located in the vicinity of such a splay fault [von Huene et al., 2020]. The terraces are less developed in the Eastern Sanak Basin and did not develop further east than the Sanak Basin (Figure 1B). They only appear between the landward-dipping normal faults, where they exist, and the BSFZ, and may be another morphological hint at preferential slip on the shallow interface and/or the near trench splay faults, again vanishing when the sutures are too far from the trench.

5.5. *The role of fluids?*

The Chugach-Prince William suture is also present in the Semidi segment but there are no trench-parallel half graben basins there, which, as discussed, could indicate that the suture zone is too far from the trench. Another solution would involve variation of additional properties besides the need of a pre-existing fault. Indeed, many other parameters are varying from the Shumagin to the Semidi segment of the AASZ, like for instance elastic coupling and fluid release, in relation with properties of the downgoing plate.

The subducting oceanic plate fabric shows contrasting orientations (Figure 11): (1) ~E–W oriented ridge fabric formed at the Kula–Pacific extinct spreading center [Byrne, 1979, Lonsdale, 1988], sub-parallel to the trench, dominate west of the Shumagin segment, while (2) ~N–S oriented ridge fabric formed at the Vancouver-Pacific or Farallon-Pacific extinct spreading center [Atwater and Menard, 1970, Stock and Molnar, 1988] prevail to the east. This abrupt variation in the plate fabric relates to the presence of a fossil triple junction located at the eastern boundary of the Shumagin segment [Stock and Molnar, 1988]. Shillington et al. [2015] show an increase in present-day bending-related extension within the incoming plate toward the west, where the trench sub-parallel Kula–Pacific oceanic fabric (Figure 1A) normal faults can be easily reactivated [Aubouin et al., 1981, Masson, 1991, Billen et al., 2007]. These western, highly faulted areas correlate with a reduction in P-wave velocity interpreted to be due to hydration of the crust and upper mantle. The background plate-interface seismicity may in turn be affected when fluids are released and migrates to the plate interface [Shillington et al., 2015, Acquisto et al., 2022]. Li et al. [2018] also image an increase in the subducting sedimentary layer thickness from west to east towards the Semidi segment, where thicker Zodiac Fan sediments [Stevenson et al., 1983] are subducting. More sediments and less bend faulting towards the eastern Semidi segment may contribute to a net decrease in plate roughness and favour increased plate interface locking and reduced background seismicity [Ruff, 1989, Wang and Bilek, 2014, Lallemand et al., 2018].

In Japan, fluids have been collected around the Tohoku landward-dipping normal fault [Sano et al., 2014] and geochemical analyses show that these come from the plate interface through the fault [Sano et al., 2014, Park et al., 2021], potentially reducing the friction [McKenzie and Jackson, 2012]. Since more fluids from the downgoing plate may be released from the Shumagin to the Unimak segment, it is a factor that may be essential in the activity of the landward-dipping normal faults and that may also participate in the weakness of the partitioning faults.

6. Conclusion

In this reappraisal of the forearc structures in the transition zone between Aleutian and Alaskan subduction zones using legacy and modern seismic data, we show that the Central Sanak basin likely localizes the onset of Aleutian strain partitioning, in agreement with plate convergence obliquity extracted from thrust earthquake rake vectors. The trench-parallel extension rate is estimated from the finite deformation to be small (less than 1 mm/yr) lower than or close to the resolution of the available, non conclusive GPS measurements.

This onset of Aleutian strain partitioning is another transitional feature between Alaskan and Aleutian subduction zones, in addition to slab dip, downgoing plate fabric orientation, trench sedimentation. We review the other forearc structures and their potential link with the subduction zone interface behaviour and segmentation. Trench perpendicular extension localising on landward-dipping normal faults may be linked to tsunamigenic shallow coseismic slip only if such normal faults feature very low friction, which we interpret geologically as reactivation of pre-existing and potentially fluid-rich structures within the terranes. This study aims to emphasise the perennial importance of mapping geological structures to better assess the seismogenic behaviour of subduction zones, in addition to modern instrumentation.

Conflicts of interest

Authors have no conflict of interest to declare.

Acknowledgements

We thank Jeff Freymueller and an anonymous reviewer for their very useful comments. Reflection images resulting from basic processing of most legacy profiles are available in the GeoMapApp database (https://www.geomapapp.org/) and the US Geological Survey (USGS) data portal (https://walrus.wr.usgs.gov/namss/search/). Data from the 1994 R/V Maurice Ewing survey EW9409 [McGeary et al., 2018] and from MGL1110 (ALEUT cruise) are available from the Marine Geoscience Data System (MGDS) data portal (https://www.marine-geo.org/tools/new_search/search_map.php).

Supplementary data

Supporting information for this article is available on the journal's website under https://doi.org/10.5802/crgeos.225 or from the author.

References

Acquisto, T., Bécel, A., Singh, S. C., and Carton, H. (2022). Evidence of strong upper oceanic crustal hydration outboard the Alaskan and Sumatran subduction zones. *J. Geophys. Res.: Solid Earth*, 127(10), article no. e2022JB024751.

Andersen, O., Knudsen, P., and Stenseng, L. (2015). The DTU13 MSS (Mean Sea Surface) and MDT (Mean Dynamic Topography) from 20 years of satellite altimetry. In Jin, S. and Barzaghi, R., editors, *IGFS 2014. International Association of Geodesy Symposia*, volume 144. Springer, Cham.

Atwater, T. and Menard, H. W. (1970). Magnetic lineations in the Northeast Pacific. *Earth Planet. Sci. Lett.*, 7, 445–450.

Aubouin, J., Bourgois, J., and Azéma, J. (1984). A new type of active margin: the convergent-extensional margin, as exemplified by the Middle America Trench off Guatemala. *Earth Planet. Sci. Lett.*, 67, 211–218.

Aubouin, J., Stephan, J. F., Renard, V., Roump, J., and Lonsdale, P. (1981). Subduction of the cocos plate in the Mid America Trench. *Nature*, 294, 146–150.

Avé Lallemant, H. G. (1996). Displacement partitioning and arc-parallel extension in the Aleutian volcanic island arc. *Tectonophysics*, 256, 279–293.

Avé Lallemant, H. G. and Guth, L. R. (1990). Role of extensional tectonics in exhumation of eclogites and blueschists in an oblique subduction setting: Northeastern Venezuela. *Geology*, 18, 950–953.

Avé Lallemant, H. G. and Oldow, J. S. (2000). Active displacement partitioning and arc-parallel extension of the Aleutian volcanic arc based on Global Positioning System geodesy and kinematic analysis. *Geology*, 28, 739–742.

Basile, C. and Brun, J. P. (1999). Transtensional faulting patterns ranging from pull-apart basins to transform continental margins: an experimental investigation. *J. Struct. Geol.*, 21, 23–37.

Bassett, D. and Watts, A. B. (2015). Gravity anomalies, crustal structure, and seismicity at subduction zones: 2. Interrelationships between fore-arc structure and seismogenic behavior. *Geochem. Geophys. Geosyst.*, 16, 1541–1576.

Bécel, A., Shillington, D. J., Delescluse, M., Nedimović, M. R., Abers, G. A., Saffer, D. M., Webb, S. C., Keranen, K. M., Roche, P.-H., Li, J., et al. (2017). Tsunamigenic structures in a creeping section of the Alaska subduction zone. *Nat. Geosci.*, 10, 609–613.

Beck, M. E. (1983). On the mechanism of tectonic transport in zones of oblique subduction. *Tectonophysics*, 93, 1–11.

Billen, M., Cowgill, E., and Buer, E. (2007). Determination of fault friction from reactivation of abyssal-hill faults in subduction zones. *Geology*, 35(9), 819–822.

Briggs, R., Witter, R., Freymueller, J., Ross, S., and Thio, H. K. (2023). Updates to the subduction interface portion of the Alaska 2023 USGS National Seismic Hazard Model. In *USGS Subduction Zone Science Workshop (Poster), January 10–11, 2023, Seattle, Washington*.

Bruhn, R. L., Pavlis, T. L., Plafker, G., and Serpa, L. (2004). Deformation during terrane accretion in the Saint Elias orogen, Alaska. *GSA Bull.*, 116(7–8), 771–787.

Bruns, T. R., von Huene, R. C. C., Lewis, S. D., and Ladd, J. W. (1987). Geology and petroleum potential of the Shumagin Margin, Alaska. In Scholl, D. W., Grantz, A., and Vedder, J. G., editors, *Geology and Resource Potential of the Western North America and Adjacent Ocean Basins: Beaufort Sea to Baja California*, Earth Science Series, 6, pages 157–189. Circum-Pacific Council for Energy and Mineral Resources, Houston, Texas.

Byrne, T. (1979). Late Paleocene demise of the Kula-Pacific spreading center. *Geology*, 7, 341–344.

Calvès, G., Auguy, C., De Lavaissière, L., Brusset, S., Calderon, Y., and Baby, P. (2017). Fore-arc seafloor unconformities and geology: Insight from 3-D seismic geomorphology analysis, Peru. *Geochem. Geophys. Geosyst.*, 18(8), article no. 30623077.

Carver, G., Sauber, J., Lettis, W., Witter, R., Whitney, B., Freymueller, J., Haeussler, P., Wesson, R., and Ekström, G. (2008). Active faults on northeastern Kodiak Island, Alaska. In Freymueller, J. T., Haeussler, P. J., Wesson, R. L., and Ekström, G., editors, *Active Tectonics and Seismic Potential of Alaska*, American Geophysical Union Geophysical Monograph, pages 167–184. American Geophysical Union, Washington, DC.

Chanier, F., Ferrière, J., and Angelier, J. (1999). Extensional deformation across an active margin, relation with subsidence, uplift, and rotations: The Hikurangi subduction, New Zealand. *Tectonics*, 18, 862–876.

Clift, P. and Vannucchi, P. (2004). Controls on tectonic accretion versus erosion in subduction zones: Implications for the origin and recycling of the continental crust. *Rev. Geophys.*, 42, 1–31.

Coney, P. J., Jones, D. L., and Monger, J. W. H. (1980). Cordilleran suspect terranes. *Nature*, 288, 329–333.

Cross, R. S. and Freymueller, J. T. (2008). Evidence for and implications of a Bering plate based on geodetic measurements from the Aleutians and western Alaska. *J. Geophys. Res.: Solid Earth*, 113, article no. B07405.

Cubas, N., Barnes, C., and Maillot, B. (2013). Inverse method applied to a sand wedge: Estimation of friction parameters and uncertainty analysis. *J. Struct. Geol.*, 55, 101–113.

Dahlen, F. A., Suppe, J., and Davis, D. (1984). Mechanics of fold-and-thrust belts and accretionary wedges: Cohesive Coulomb theory. *J. Geophys. Res.*, 89, 87–101.

Davies, J., Sykes, L., House, L., and Jacob, K. (1981). Shumagin seismic gap, Alaska Peninsula: History of great earthquakes, tectonic setting, and evidence for high seismic potential. *J. Geophys. Res.: Solid Earth*, 86, 3821–3855.

Davis, G. A., Monger, J. W. H., and Burchfiel, B. C. (1978). Mesozoic construction of the Cordilleran "collage," central British Columbia to central California. In Howell, D. G. and McDougall, K. A., editors, *Mesozoic Paleogeography of the Western United States. Pacific Coast Paleogeography Symposium*, volume 2, pages 1–32. Society Economic Paleontologists Mineralogists, Pacific Section, Los Angeles, California.

DeMets, C. (1992). Oblique Convergence and Deformation Along the Kuril and Japan Trenches. *J. Geophys. Res.-Solid Earth*, 97, 17615–17625.

Dickinson, W. R. (2004). Evolution of the North American Cordillera. *Annu. Rev. Earth Planet. Sci.*, 32, 13–45.

Dominguez, S., Lallemand, S. E., Malavieille, J., and

von Huene, R. (1998). Upper plate deformation associated with seamount subduction. *Tectonophysics*, 293, 207–224.

Dung, N. K. and Thanh, D. D. (2016). Using the Analytic Signal method of gravity gradient tensor (GGT) to determine the location and depth of the faults in the pre-Cenozoic basement rocks of the Red River Trough. *Vietnam J. Earth Sci.*, 38, 143–152.

Dziewonski, A. M., Chou, T.-A., and Woodhouse, J. H. (1981). Determination of earthquake source parameters from waveform data for studies of global and regional seismicity. *J. Geophys. Res.*, 86(B4), 2825–2852.

Ekström, G. and Engdahl, E. R. (1989). Earthquake source parameters and stress distribution in the Adak Island region of the central Aleutian Islands, Alaska. *J. Geophys. Res.: Solid Earth*, 94(B11), 15499–15519.

Ekström, G., Nettles, M., and Dziewoński, A. M. (2012). The global CMT project 2004–2010: Centroid-moment tensors for 13,017 earthquakes. *Phys. Earth Planet. Inter.*, 200–201, 1–9.

Elliott, J. and Freymueller, J. T. (2020). A Block Model of Present-Day Kinematics of Alaska and Western Canada. *J. Geophys. Res.: Solid Earth*, 125(7), article no. e2019JB018378.

Finzel, E. S., Flesch, L. M., and Ridgway, K. D. (2011). Kinematics of a diffuse North America-Pacific-Bering plate boundary in Alaska and western Canada. *Geology*, 39, 835–838.

Finzel, E. S., Flesch, L. M., Ridgway, K. D., Holt, W. E., and Ghosh, A. (2015). Surface motions and intraplate continental deformation in Alaska driven by mantle flow. *Geophys. Res. Lett.*, 42, 4350–4358.

Fisher, M. A. (1981). Location of the Border Ranges fault southwest of Kodiak Island, Alaska. *Geol. Soc. Am. Bull.*, 92(1), 19–30.

Fitch, T. J. (1972). Plate convergence, transcurrent faults, and internal deformation adjacent to Southeast Asia and the Western Pacific. *J. Geophys. Res.*, 77, 4432–4460.

Fournier, T. J. and Freymueller, J. T. (2007). Transition from locked to creeping subduction in the Shumagin region, Alaska. *Geophys. Res. Lett.*, 34, article no. L06303.

Garver, J. I. and Davidson, C. (2017). Accretion and Translation of the Chugach, Prince William, and Yakutat terranes in Alaska. In *Geological Society of America Abstracts with Programs*, volume 49, No. 6.

Geist, E. L., Childs, J. R., and Scholl, D. W. (1988). The origin of summit basins on the Aleutian Ridge: implications for block rotation of an arc massif. *Tectonics*, 7, 327–341.

Hayes, G. P., Moore, G. L., Portner, D. E., Hearne, M., Flamme, H., Furtney, M., and Smoczyk, G. M. (2018). Slab2, a comprehensive subduction zone geometry model. *Science*, 362, 58–61.

Horowitz, W. L., Steffy, D. A., and Hoose, P. J. (1989). Geologic report for the Shumagin Planning Area, Western Gulf of Alaska. Technical Report MMS 89-0097, U.S. Department of the Interior, Minerals Management Service, Alaska OCS Region, https://www.boem.gov/oil-gas-energy/890097.

Huchon, P. and Le Pichon, X. (1984). Sunda Strait and central Sumatra fault. *Geology*, 12(11), 668–672.

Hyndman, R. D., Yamano, M., and Oleskevich, D. A. (1997). The seismogenic zone of subduction thrust faults. *Island Arc*, 6, 244–260.

Ide, S., Baltay, A., and Beroza, G. C. (2011). Shallow dynamic overshoot and energetic deep rupture in the 2011 Mw 9.0 Tohoku-Oki earthquake. *Science*, 332, 1426–1429.

Jarrard, R. D. (1986). Terrane motion by strike-slip faulting of forearc slivers. *Geology*, 14, 780–783.

Jiang, Y., González, P. J., and Bürgmann, R. (2022). Subduction earthquakes controlled by incoming plate geometry: The 2020 M> 7.5 Shumagin, Alaska, earthquake doublet. *Earth Planet. Sci. Lett.*, 584, article no. 117447.

Johnson, J. M. and Satake, K. (1997). Estimation of seismic moment and slip distribution of the April 1, 1946, Aleutian tsunami earthquake. *J. Geophys. Res.*, 102, 11765–11774.

Kanamori, H. (1972). Mechanism of tsunami earthquakes. *Phys. Earth Planet. Inter.*, 6, 346–359.

Kelleher, J. and McCann, W. (1976). Buoyant zones, great earthquakes, and unstable boundaries of subduction. *J. Geophys. Res.*, 81, 4885–4896.

Kimura, G. (1986). Oblique subduction and collision: Forearc tectonics of the Kuril Arc. *Geology*, 14, 404–407.

Kreemer, C., Blewitt, G., and Klein, E. C. (2014). A geodetic plate motion and global strain rate model. *Geochem. Geophys. Geosyst.*, 15, 3849–3889.

Kuehn, H. (2019). *Along-trench segmentation and down-dip limit of the seismogenic zone at the eastern Alaska-Aleutian subduction zone*. PhD thesis, Dalhousie University.

Kuramoto, S. and Konishi, K. (1989). The Southwest Ryukyu Arc is a migrating microplate (forearc sliver). *Tectonophysics*, 163, 75–91.

Lallemand, S., Peyret, M., Rijsingen, E., Arcay, D., and Heuret, A. (2018). Roughness characteristics of oceanic seafloor prior to subduction in relation to the seismogenic potential of subduction zones. *Geochem. Geophys. Geosyst.*, 19, 2121–2146.

Lallemand, S. E., Schnurle, P., and Malavieille, J. (1994). Coulomb theory applied to accretionary and non accretionary wedges: Possible causes for tectonic erosion and/or frontal accretion. *J. Geophys. Res.-Solid Earth*, 99, 12033–12055.

Le Pichon, X., Henry, P., and Lallemant, S. (1993). Accretion and erosion in subduction zones: The role of fluids. *Annu. Rev. Earth Planet. Sci.*, 21, 307–331.

Lewis, S. D., Ladd, J. W., and Bruns, T. R. (1988). Structural development of an accretionary prism by thrust and strike-slip faulting: Shumagin region, Aleutian Trench. *Geol. Soc. Am. Bull.*, 100, 767–782.

Li, J., Shillington, D. J., Saffer, D. M., Bécel, A., Nedimović, M. R., Kuehn, H., Webb, S. C., Keranen, K. M., and Abers, G. A. (2018). Connections between subducted sediment, pore-fluid pressure, and earthquake behavior along the Alaska megathrust. *Geology*, 46, 299–302.

Li, S., Freymueller, J., and McCaffrey, R. (2016). Slow slip events and time-dependent variations in locking beneath Lower Cook Inlet of the Alaska-Aleutian subduction zone. *J. Geophys. Res.-Solid Earth*, 121, 1060–1079.

Li, S. and Freymueller, J. T. (2018). Spatial variation of slip behavior beneath the Alaska Peninsula along Alaska-Aleutian subduction zone. *Geophys. Res. Lett.*, 45, 3453–3460.

Liang, Y., Delescluse, M., Qiu, Y., Pubellier, M., Chamot-Rooke, N., Wang, J., Nie, X., Watremez, L., Chang, S., Pichot, T., Savva, D., and Meresse, F. (2019). Décollements, detachments, and rafts in the extended crust of dangerous ground, South China sea: The role of inherited contacts. *Tectonics*, 38, 1863–1883.

Liu, C., Lay, T., and Xiong, X. (2022). The 29 July 2021 MW 8.2 Chignik, Alaska Peninsula earthquake rupture inferred from seismic and geodetic observations: Re-Rupture of the Western 2/3 of the 1938 Rupture Zone. *Geophys. Res. Lett.*, 49, article no. e2021GL096004.

Liu, C., Lay, T., Xiong, X., and Wen, Y. (2020). Rupture of the 2020 Mw 7.8 earthquake in the Shumagin Gap inferred from seismic and geodetic observations. *Geophys. Res. Lett.*, 47, article no. e2020GL090806.

Lizarralde, D., Holbrook, W. S., McGeary, S., Bangs, N. L., and Diebold, J. B. (2002). Crustal construction of a volcanic arc, wide-angle seismic results from the western Alaska Peninsula. *J. Geophys. Res.: Solid Earth*, 107, article no. EPM-4.

Lonsdale, P. (1988). Paleogene history of the Kula plate: Offshore evidence and onshore implications. *Geol. Soc. Am. Bull.*, 100, 733–754.

López, A. M. and Okal, E. A. (2006). A seismological reassessment of the source of the 1946 Aleutian 'tsunami' earthquake. *Geophys. J. Int.*, 165, 835–849.

Marlow, M. S. and Cooper, A. K. (1980). Mesozoic and Cenozoic structural trends under southern Bering Sea shelf. *AAPG Bull.*, 64, 2139–2155.

Masson, D. G. (1991). Fault patterns at outer trench walls. *Mar. Geophys. Res.*, 13, 209–225.

McCaffrey, R. (1992). Oblique plate convergence, slip vectors, and forearc deformation. *J. Geophys. Res.: Solid Earth*, 97, 8905–8915.

McCaffrey, R. (1996). *Slip Partitioning at Convergent Plate Boundaries of SE Asia*, volume 106(1) of *Geological Society, London, Special Publications*. Geological Society of London.

McClay, K. and Dooley, T. (1995). Analogue models of pull-apart basins. *Geology*, 23(8), 711–714.

McGeary, S., Bangs, N. L., Bond, G., and Diebold, J. B. (2018). *Processed multichannel seismic data along the Aleutian arc and the extensive Alaskina continental shelf, acquired during the R/V Maurice Ewing survey EW9409 (1994)*. Interdisciplinary Earth Data Alliance (IEDA), https://www.iedadata.org/.

McKenzie, D. and Jackson, J. (2012). Tsunami earthquake generation by the release of gravitational potential energy. *Earth Planet. Sci. Lett.*, 345, 1–8.

Mickus, K. L. and Hinojosa, J. H. (2001). The complete gravity gradient tensor derived from the verti-

cal component of gravity: a Fourier transform technique. *J. Appl. Geophys.*, 46, 159–174.

Miller, J. J., von Huene, R. E., and Ryan, H. F. (2014). The 1946 Unimak tsunami earthquake area: revised tectonic structure in reprocessed seismic images and a suspect near field tsunami source. Open-File Report 2014-1024, US Department of the Interior, US Geological Survey.

Monger, J. and Irving, E. (1980). Northward displacement of north-central British Columbia. *Nature*, 285, 289–294.

Moore, J. C. (1973). Cretaceous continental margin sedimentation, Southwestern Alaska. *Geol. Soc. Am. Bull.*, 84, 595–614.

Moore, J. C. (1974). *Geological and Structural Map of the Sanak Island, Southwestern Alaska*. United States Geological Survey, IMAP 817.

Moore, J. C., Byrne, T., Plumley, P. W., Reid, M., Gibbons, H., and Coe, R. S. (1983). Paleogene evolution of the Kodiak Islands, Alaska: Consequences of ridge-trench interaction in a more southerly latitude. *Tectonics*, 2(3), 265–293.

Noda, A. (2016). Forearc basins: Types, geometries, and relationships to subduction zone dynamics. *GSA Bull.*, 128(5–6), 879–895.

Okal, E. A. and Hébert, H. (2007). Far-field simulation of the 1946 Aleutian tsunami. *Geophys. J. Int.*, 169, 1229–1238.

Oleskevich, D. A., Hyndman, R. D., and Wang, K. (1999). The updip and downdip limits to great subduction earthquakes: Thermal and structural models of Cascadia, south Alaska, SW Japan, and Chile. *J. Geophys. Res.*, 104(B7), 14965–14991.

Park, J.-O., Tsuru, T., Fujie, G., Jamali Hondori, E., Kagoshima, T., Takahata, N., Zhao, D., and Sano, Y. (2021). Seismic reflection images of possible mantle-fluid conduits and basal erosion in the 2011 Tohoku earthquake rupture area. *Front. Earth Sci.*, 9, article no. 687382.

Plafker, G. and Berg, H. C. (1994). Overview of the geology and tectonic evolution of Alaska. In Plafker, G. and Berg, H. C., editors, *The Geology of North America*, volume G-1, pages 989–1021. Geological Society of America, Boulder.

Plafker, G., Moore, J. C., and Winkler, G. R. (1994). Geology of the southern Alaska margin. In Plafker, G. and Berg, H. C., editors, *The Geology of North America*, volume G-1, pages 389–449. Geological Society of America, Boulder.

Pubellier, M. and Cobbold, P. R. (1996). Analogue models for the transpressional docking of volcanic arcs in the Western Pacific. *Tectonophysics*, 253, 33–52.

Pubellier, M., Quebral, R., Aurelio, M., and Rangin, C. (1996). *Docking and Post-docking Escape Tectonics in the Southern Philippines*. Geological Society London Special Publications. Geological Society of London, London.

Ratzov, G., Collot, J.-Y., Sosson, M., and Migeon, S. (2010). Mass transport deposits in the northern Ecuador subduction trench: Result of frontal erosion over multiple seismic cycles. *Earth Planet. Sci. Lett.*, 296(1–2), 89–102.

Ruff, L. (1989). Do trench sediments affect great earthquake occurrence in subduction zones? *Pure Appl. Geophys.*, 129(1–2), 263–282.

Ryan, H. F. and Scholl, D. W. (1989). The evolution of forearc structures along an oblique convergent margin, Central Aleutian Arc. *Tectonics*, 8, 497–516.

Ryan, W. B. F., Carbotte, S. M., Coplan, J., O'Hara, S., Melkonian, A., Arko, R., Weissel, R. A., Ferrini, V., Goodwillie, A., Nitsche, F., Bonczkowski, J., and Zemsky, R. (2009). Global Multi-Resolution Topography (GMRT) synthesis data set. *Geochem. Geophys. Geosyst.*, 10, article no. Q03014.

Saad, A. H. (2006). Understanding gravity gradients—a tutorial. *Lead. Edge*, 25, 942–949.

Sano, Y., Hara, T., Takahata, N., Kawagucci, S., Honda, M., Nishio, Y., Tanikawa, W., Hasegawa, A., and Hattori, K. (2014). Helium anomalies suggest a fluid pathway from mantle to trench during the 2011 Tohoku-Oki earthquake. *Nat. Commun.*, 5, article no. 3084.

Schlüter, H. U., Gaedicke, C., Roeser, H. A., Schreckenberger, B., Meyer, H., Reichert, C., Djajadihardja, Y., and Prexl, A. (2002). Tectonic features of the southern Sumatra-western Java forearc of Indonesia. *Tectonics*, 21(5), article no. 1047.

Scholl, D. W., Buffington, E. C., and Marlow, M. S. (1975). Plate tectonics and the Structural Evolution of the Aleutian-Bering Sea Region. *Geol. Soc. Am. Spec. Pap.*, 151, 1–32.

Scholl, D. W., Vallier, T. L., and Stevenson, A. J. (1987). Geologic evolution and petroleum geology of the Aleutian Ridge. In Scholl, D. W., Grantz, A., and Vedder, J. G., editors, *Geology and Resource Potential of the Continental Margin of Western North*

America and Adjacent Ocean Basins: Beaufort Sea to Baja California, Earth Science Series, 6, pages 123–156. Circum-Pacific Council for Energy and Mineral Resources, Houston, Texas.

Schütt, J. M. and Whipp, D. M. (2020). Controls on continental strain partitioning above an oblique subduction zone, Northern Andes. *Tectonics*, 39, 1–21.

Shillington, D. J., Bécel, A., and Nedimović, M. R. (2022). Upper plate structure and megathrust properties in the shumagin gap near the July 2020 M7.8 Simeonof event. *Geophys. Res. Lett.*, 49, article no. e2021GL096974.

Shillington, D. J., Bécel, A., Nedimović, M. R., Kuehn, H., Webb, S. C., Abers, G. A., Keranen, K. M., Li, J., Delescluse, M., and Mattei-Salicrup, G. A. (2015). Link between plate fabric, hydration and subduction zone seismicity in Alaska. *Nat. Geosci.*, 8, 961–964.

Shillington, D. J., Nedimović, M. R., Webb, S., Bécel, A., Delescluse, M., Li, J., Kuehn, H., Biescas, B., Wessbecher, A., Farkas, A., Eddy, C., Hostetler, K., Perls, H., Zietman, J., Keranen, K., and Louden, K. (2011). Constraints on the Aleutian subduction zone from the Shumagin gap to Kodiak asperity from new MCS and OBS data of the ALEUT Project. In *AGU Fall Meeting Abstracts 2011*. AGU, Washington DC. T33A-2387.

Song, T.-R. A. and Simons, M. (2003). Large trench-parallel gravity variations predict seismogenic behavior in subduction zones. *Science*, 301, 630–633.

Stevenson, A. J., Scholl, D. W., and Vallier, T. L. (1983). Tectonic and geologic implications of the Zodiac fan, Aleutian Abyssal Plain, northeast Pacific. *Geol. Soc. Am. Bull.*, 94, 259–273.

Stock, J. and Molnar, P. (1988). Uncertainties and implications of the Late Cretaceous and Tertiary position of North America relative to the Farallon, Kula, and Pacific Plates. *Tectonics*, 7, 1339–1384.

Tape, C. and Lomax, A. (2022). Aftershock regions of Aleutian-Alaska megathrust earthquakes, 1938–2021. *J. Geophys. Res.*, 127, article no. e2022JB024336.

Tsuji, T., Ito, Y., Kido, M., Osada, Y., Fujimoto, H., Ashi, J., Kinoshita, M., and Matsuoka, T. (2011). Potential tsunamigenic faults of the 2011 off the Pacific coast of Tohoku Earthquake. *Earth Planets Space*, 63, article no. 58.

Tsuji, T., Kawamura, K., Kanamatsu, T., Kasaya, T., Fujikura, K., Ito, Y., Tsuru, T., and Kinoshita, M. (2013). Extension of continental crust by anelastic deformation during the 2011 Tohoku-oki earthquake: The role of extensional faulting in the generation of a great tsunami. *Earth Planet. Sci. Lett.*, 364, 44–58.

Vallier, T. L., Scholl, D. W., Fisher, M. A., Bruns, T. R., Wilson, F. H., von Huene, R., and Stevenson, A. J. (1994). Geologic Framework of the Aleutian Arc, Alaska. In Plafker, G. and Berg, H. C., editors, *The Geology of North America*, volume G-1, pages 367–388. Geological Society of America, Boulder.

von Huene, R. and La Verne, D. K. (1973). Tectonic Summary of Leg 180. In Kulm, L. D., von Huene, R., et al., editors, *Initial Reports of the Deep Sea Drilling Project*, volume 18, pages 961–976. Texas A & M University, Texas, http://sedis.iodp.org/pub-catalogue/index.php?id=10.2973/dsdp.proc.18.133.1973.

von Huene, R. and Lallemand, S. (1990). Tectonic erosion along the Japan and Peru convergent margins. *Geol. Soc. Am. Bull.*, 102, 704–720.

von Huene, R., Miller, J. J., and Dartnell, P. (2016). A possible transoceanic tsunami directed toward the US west coast from the Semidi segment, Alaska convergent margin. *Geochem. Geophys. Geosyst.*, 17(3), 645–659.

von Huene, R., Miller, J. J., and Krabbenhoeft, A. (2019). The Shumagin seismic gap structure and associated tsunami hazards, Alaska convergent margin. *Geosphere*, 15, 324–341.

von Huene, R., Miller, J. J., and Krabbenhoeft, A. (2020). The Alaska convergent margin backstop splay fault zone, a potential large tsunami generator between the frontal prism and continental framework. *Geochem. Geophys. Geosyst.*, 22(1), article no. e2019GC008901.

von Huene, R., Miller, J. J., and Weinrebe, W. (2012). Subducting plate geology in three great earthquake ruptures of the western Alaska margin, Kodiak to Unimak. *Geosphere*, 8(3), 628–644.

von Huene, R. and Scholl, D. W. (1991). Observations at convergent margins concerning sediment subduction, subduction erosion, and the growth of continental crust. *Rev. Geophys.*, 29, 279–316.

Wang, K. and Bilek, S. L. (2014). Fault creep caused by subduction of rough seafloor relief. *Tectonophysics*, 610, 1–24.

Wells, R. E., Blakely, R. J., Sugiyama, Y., Scholl, D. W., and Dinterman, P. A. (2003). Basin-centered asperities in great subduction zone earthquakes: A link between slip, subsidence, and subduction erosion? *J. Geophys. Res. Solid Earth*, 108(B10), article no. 2507.

Worrall, D. M. (1991). Tectonic history of the Bering Sea and the evolution of Tertiary strike-slip basins of the Bering Shelf. Geological Society of America Special Papers 257, page 120.

Xue, X. and Freymueller, J. T. (2020). A 25-year history of volcano magma supply in the east central Aleutian arc, Alaska. *Geophys. Res. Lett.*, 47, article no. e2020GL088388.